Tornadoes and Downbursts in the Context of Generalized Planetary Scales

T. THEODORE FUJITA

Reprinted from JOURNAL OF THE ATMOSPHERIC SCIENCES, Vol. 38, No. 8, August 1981
American Meteorological Society
Printed in U. S. A.

Reprinted from JOURNAL OF THE ATMOSPHERIC SCIENCES, Vol. 38, No. 8, August 1981
American Meteorological Society
Printed in U. S. A.

Tornadoes and Downbursts in the Context of Generalized Planetary Scales

T. THEODORE FUJITA

Department of Geophysical Sciences, The University of Chicago, Chicago, IL 60637

(Manuscript received 24 December 1980, in final form 2 February 1981)

ABSTRACT

In order to cover a wide range of horizontal dimensions of airflow, the author proposes a series of five scales, maso, meso, miso (to be read as my-so), moso and muso arranged in the order of the vowels, A, E, I, O, U. The dimensions decrease by two orders of magnitude per scale, beginning with the planet's equator length chosen to be the maximum dimension of masoscale for each planet.

Mesoscale highs and lows were described on the basis of mesoanalyses, while sub-mesoscale disturbances were depicted by cataloging over 20 000 photographs of wind effects taken from low-flying aircraft during the past 15 years. Various motion thus classified into these scales led to a conclusion that extreme winds induced by thunderstorms are associated with misoscale and mososcale airflow spawned by the parent, mesoscale disturbances.

1. Historical overview of mesoscale

The invention of the barometer led people to relate the daily weather with barometric readings; high pressure symbolizes fine weather; low pressure, bad weather; and extremely low-pressure storms. Discovery of air masses and fronts in the early 1920's by the Norwegian school altered the simple-minded pressure-weather relationship into so-called synoptic analysis, relating weather patterns with fronts and cyclones.

Local storms in continental Europe and the United States, thunderstorms in particular, are due to intense heating in warm seasons and are not always related to frontal activities. Since the 1920's, both frontal and non-frontal thunderstorms were investigated by various researchers: heat thunderstorms by Brooks (1922), cold-air production by Suckstorff (1938), thunderstorm highs by Schaffer (1947) and many others.

As air traffic increased in the 1940's, squall-line and thunderstorm-related accidents and difficulties occurred in various parts of the world. Fact-finding networks covering local areas were operated in both Germany and Japan. Some of their results had been classified until the end of the second world war. These networks were Lindenberger Böennetz (Squall Network) in 1939–41, 20 km east-southeast of Berlin reported by Koschmieder (1955) and Maebashi Raiu Kansokumo (Maebashi Thunderstorm Network) in 1940, 100 km northwest of Tokyo reported by Fujiwara (1943). The Thunderstorm Project in 1946 (Florida) and 1947 (Ohio) operated the most comprehensive data-collection networks, as reported by Byers and Braham (1949).

Severe weather events associated with small-scale disturbances, regarded as noise in daily weather analyses, became the focal point of storm researchers [a micro study by Williams (1948), pressure pulsations by Brunk (1949), a micro-analytical study by Fujita (1950), etc.].

The term meso, designating the subsynoptic noise, was first used by Ligda (1951) in emphasizing the scale of radar echoes. Since then U.S. Army Signal Corps used frequently but internally the term "mesometeorological" to identify small-scale weather phenomena which could affect the Army's operations.

Meanwhile, U.S. Weather Bureau defined the "mesoscale" to be centered between 10 and 100 mi, leading to the publications of mesometeorological papers [mesometeorological study of squall lines by Fujita (1955) and mesoanalysis by Fujita, Newstein and Tepper (1956), both with color pages].

The original mesometeorological scale was shifted to 10–100 km after the adoption of the metric system. *The Glossary of Meteorology* (1959) defines synoptic as "in general, pertaining to or affording an overall view." The key words for synoptic in meteorology are "overall" and "simultaneous" data collected for weather analyses. Petterssen (1956), applying this fundamental definition, suggested the use of "macrosynoptic", "mesosynoptic" and "microsynoptic", thus extending the concept of the conventional term "synoptic" into mesoscale and microscale.

Byers (1959) and Tepper (1959) attempted to generalize the scale of atmospheric motion through five orders of magnitude, ranging between a few tenths of a kilometer to the dimensions of long waves.

0022-4928/81/081511-24$10.00

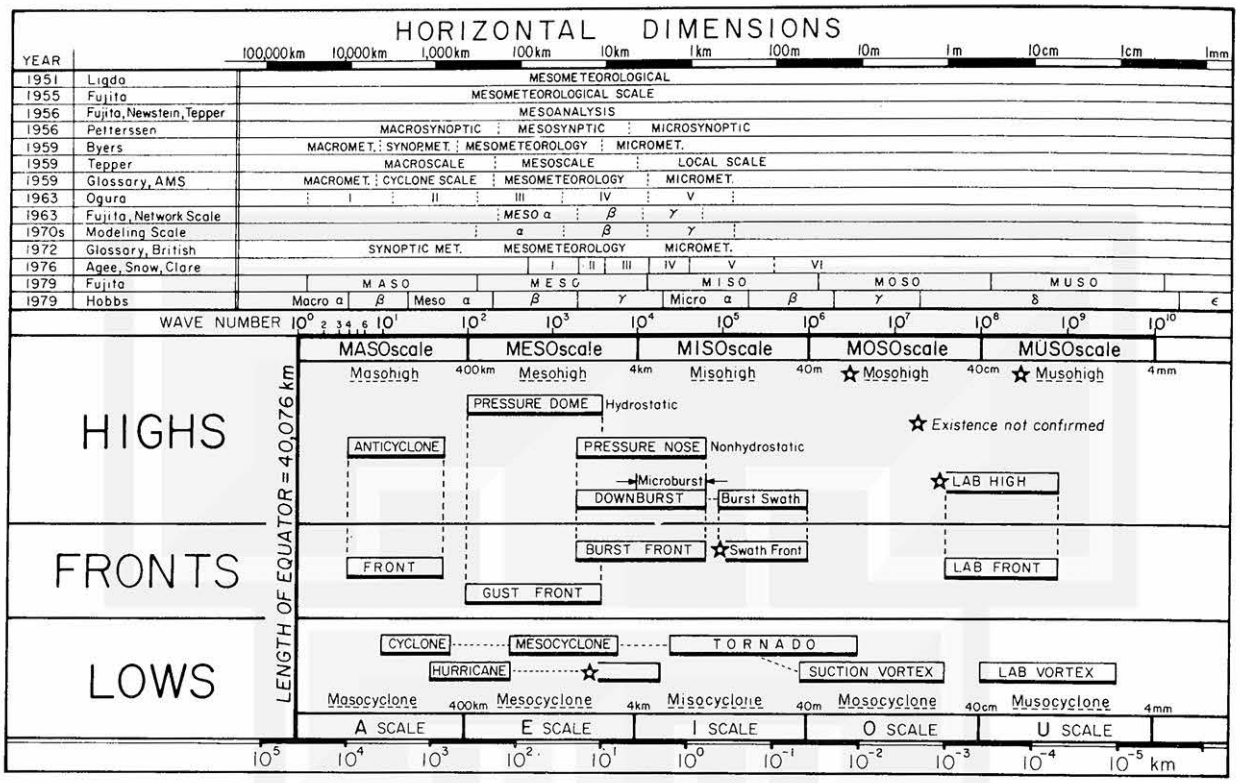

FIG. 1. A diagram showing the historical definitions of the mesoscale along with the five scales, maso-, meso-, miso-, moso- and musoscale proposed by the author.

In their articles on severe local storms, Ogura (1963) and Fujita (1963) independently suggested subclassifications of scales for every "one order of magnitude" in horizontal dimensions. Ogura's (1963) Group Numbers I, II, III, IV and V are centered at 10 000, 1000, 100, 10 and 1 km, respectively, with corresponding phenomena ranging between planetary waves to Rayleigh-type convections. Meanwhile, Fujita (1963) emphasized a need for three-density networks with station densities classified into meso-α, meso-β, and meso-γ for depicting all types of mesoscale disturbances. Currently, the grid size of numerical modeling of mesoscale phenomena is categorized into α, β, and γ which correspond to Ogura's groups III, IV and V, respectively.

The diameter of tornadoes rarely exceeds 1000 m or the meso-γ scale. Fujita[1] found that subtornado-scale vortices, called "suction vortices" orbit around the core of large tornadoes. These vortices are one order of magnitude smaller than their parent tornado. Initially, Fujita (1970) used the term "suction spot" with a remark that there are evidences that suction spots are in a state of rotation. The suspected rotation was confirmed by Fujita *et al.* (1972) on the basis of the swirl pattern of sweet-potato vines in the wake of a tornado near Tokyo, Japan.

In an attempt to accommodate the dimensions of tornadoes and suction vortices, Agee *et al.* (1976) proposed a subclassification of mesoscale into I–VI which extend through four orders of magnitude between 10 m and 100 km.

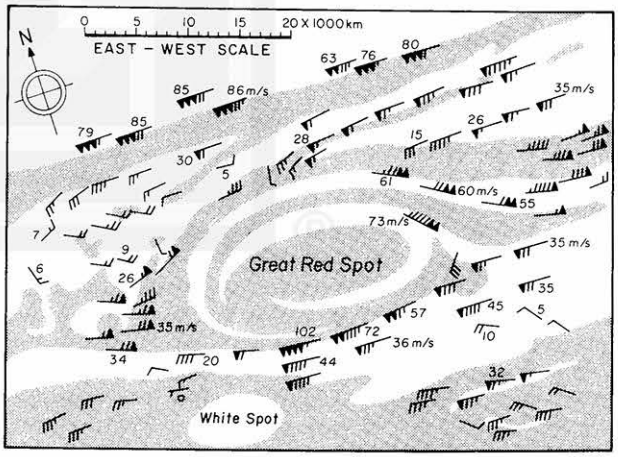

FIG. 2. Cloud-motion vectors around Jupiter's Great Red Spot, computed by the author based on four pictures taken by Voyager I on 2 and 3 February 1979.

[1] Fujita, T. T., 1971: Proposed mechanism of suction spots accompanied by tornadoes. *Preprints 7th Conf. Severe Local Storms*, Kansas City, MO, Amer. Meteor. Soc., 208–213.

Fig. 1 summarizes the geometric scales proposed by various researchers, along with both confirmed and unconfirmed disturbances associated with highs, fronts and lows. It is seen that there are two schemes of scaling atmospheric motion. The first scheme is based on the familiar sequence, macro, meso and micro with their dimensional increments, approximately two orders of magnitude each. The second scheme designates scales in either numerical or alphabetic (Greek) order. Ogura's I, II, III, . . . and meso-α, meso-β, meso-γ are separated by one order of magnitude while Agee *et al.*'s I, II, III, . . . , by nonuniform scale separations ranging between approximately one-third to one order of magnitude. The macro, meso, micro sequence of the first scheme is useful in identifying the subfields of meteorology, because each scale extends through approximately two orders of magnitudes, including a variety of important scales of motion.

By combining the mAcro-mEso-mIcro sequence with that of the five vowels in alphabetic order, Fujita[2] proposed a sequence of five scales, mAso, mEso, mIso (my-so), mOso, and mUso (myu-so). The increment of the horizontal dimensions is two orders of magnitude per scale. What has not been worked out in this sequence of scales is the dividing lines which are $10^{1/2}$, $100 \times 10^{1/2}$ km, etc., if we were to choose 10–100 km as being the center dimension of the mesoscale.

The new A-E-I-O-U scales in Fig. 1 are based on the dimension of the planet earth, so that the maximum length of mesoscale is the equator length of the earth, 40 076 km approximated as 40 000 km. The dividing dimensions of these scales are 40 000 km (masoscale), 400 km (mesoscale), 4 km (misoscale), 40 m (mososcale), 40 cm (musoscale).

High-pressure, frontal and low-pressure disturbances presented in Fig. 1 are either confirmed or unconfirmed systems which are outlined later in this paper. It should be mentioned, however, that the types of disturbances are subject to revision when new evidence and data become available in the future years.

[2] Fujita, T. T., 1979: Objectives, operation, and results of Project NIMROD. *Preprints 11th Conf. Severe Local Storms*, Kansas City, MO, Amer. Meteor. Soc., 259–266.

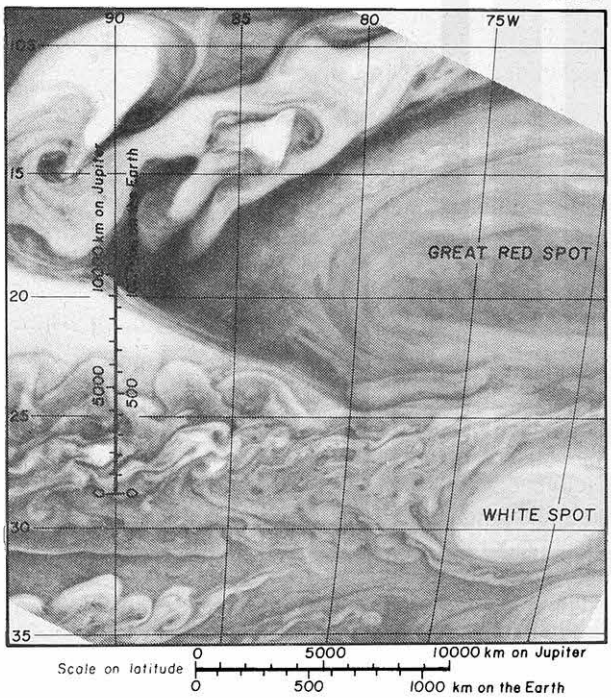

FIG. 3. Great Red Spot, a white spot and shear vortices in Jupiter's southern hemisphere. This picture was taken by Voyager I on 1 March 1979 when the spacecraft was 5 000 000 km from the planet. Most shear vortices in this photo are Jupiter's mesoscale eddies. The smallest vortices are ~100 km across. Courtesy of NASA. Grid lines and scales added by the author.

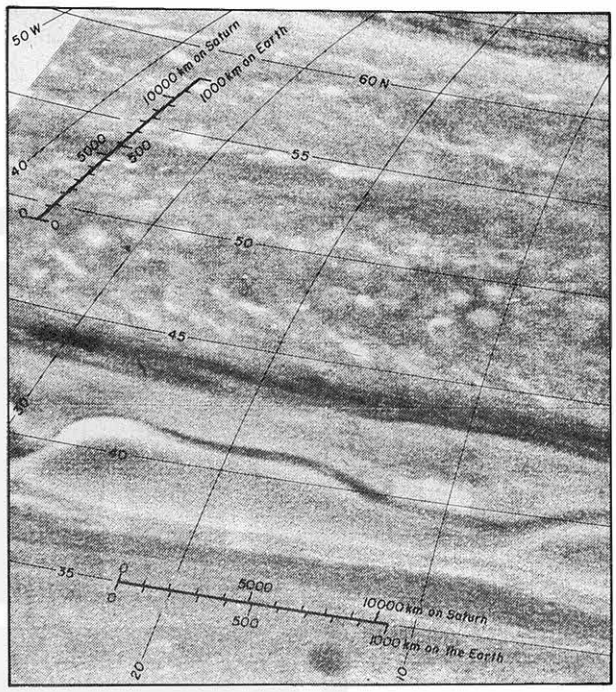

FIG. 4. Zonal waves and convection-like cells in Saturn's northern hemisphere. Picture was taken by Voyager I on 10 November 1980 when the spacecraft was 3 000 000 km from the planet. Convection cells between 45 and 60°N are 300–1 000 km (Saturn's mesoscale) in size. Courtesy of NASA. Grid lines added by the author.

2. Planetary mesoscale

Exploration of other planets in the Solar System since the 1970's provided us with the knowledge of both geographic and atmospheric scales that have not been observed by ground-based telescopes. The horizontal dimension of Jupiter's Great Red Spot is in excess of 20 000 km, yet it is no longer a spot,

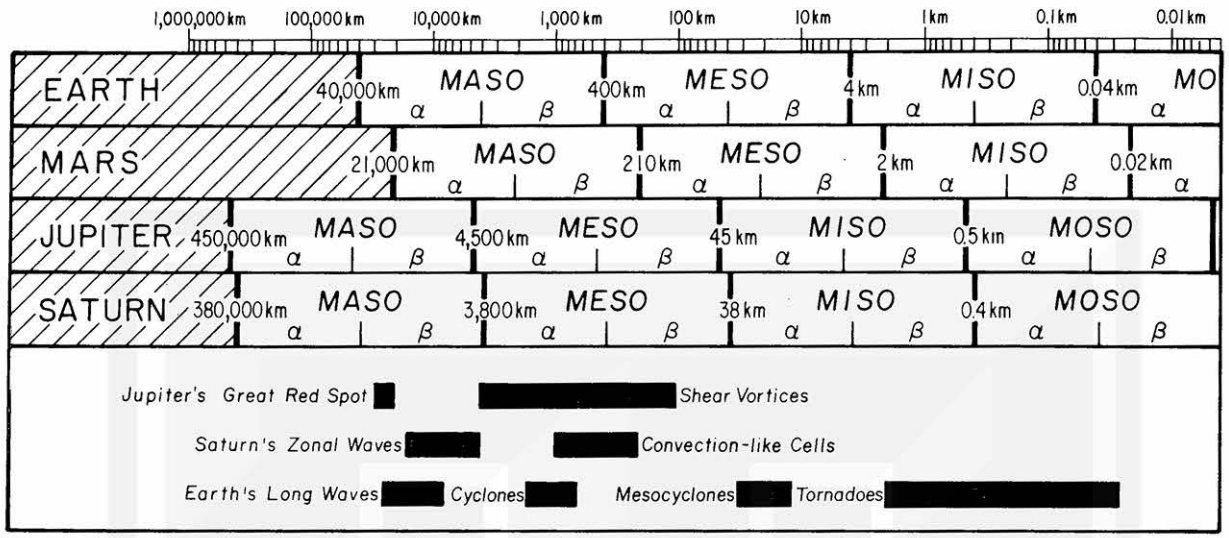

FIG. 5. Proposed scales on planets Earth, Mars, Jupiter and Saturn. The largest dimension of the masoscale is chosen as the equator length of each planet.

but a giant swirl cloud in the planet's southern hemisphere.

Successive pictures of the Spot taken during the approach phase of Voyager I were used to compute the cloud-motion vectors presented in Fig. 2. The mean relative vorticity of the anticyclonic swirl turned out to be $\sim -10^{-5}$ s^{-1}, in spite of its maximum tangential speed of 102 m s^{-1} (228 mph). Jupiter's masoscale, corresponding to wave numbers 1–100 on that planet, extends between 4480 and 448 000 km. The horizontal dimensions of the Great Red Spot (swirl) fall into Jupiter's masoscale.

Fig. 3 shows a picture of Jupiter's southern hemisphere superimposed on the longitude and latitude lines at 5° intervals. A set of two scales (km) denote true horizontal dimensions on Jupiter assumed ellipsoid and those on the earth with Jupiter's longitudes and latitudes. Numerous shear vortices on the planet, of circular or irregular shapes, are 100–5000 km across. They are Jupiter's mesocyclone with their dimensions comparable to the earth's masocyclone.

Saturn's clouds are characterized by zonal waves near 40°N and convection-like cells located between 44 and 63°N. These cells are mesoscale clouds with their shearing features which imply the existence of the maximum easterly flow in the zone centered along the 50°N latitude (Fig. 4).

So far an attempt was made to assign planetary scales based on wavenumbers on respective planets. In other words, the characteristic dimensions of planetary scales are assumed strictly proportional to the equator length. One of the main reasons for choosing the wavenumber-based scaling is that we are not able to determine the scales on other planets, which correspond to each scale on the earth. Tornadoes, for instance, are misoscale cyclones on the earth. Other planets may or may not have tornado-equivalent vortices. On the contrary, some disturbances on other planets may never be found on the earth. As a result, we are not able to determine the characteristic scale on other planets, which corresponds to a specific scale on our planet.

Each scale on each planet is expected to be characterized by its own unique disturbances, as determined by the following parameters:

1) rotation rate of the planet;
2) composition, temperature and pressure of the planetary atmosphere;
3) radiation balance, equator to poles and the surface to the top of the atmosphere.
4) upward heat flow from the surface of the planet;
5) height of the tropopause;
6) other properties such as land and sea distribution, if applicable, surface topography, if any, etc.

Practically all types of masoscale disturbances on the earth have been confirmed, while mesoscale and smaller disturbances are still being described or discovered. In general, the smaller the disturbances the shorter their lifetime, making their confirmation more difficult. Disturbances on other planets are extremely difficult to confirm because of their distances and of the limited opportunities of repeated observations. Nonetheless, the studies of different scales of motion on other planets will be of great help in understanding our own atmosphere.

Maso, meso, miso, . . . , scales applicable to four planets are presented in Fig. 5, along with the dimensions of selected disturbances on three planets. For the convenience of identifying the subscales separated by one order of magnitude, each of the

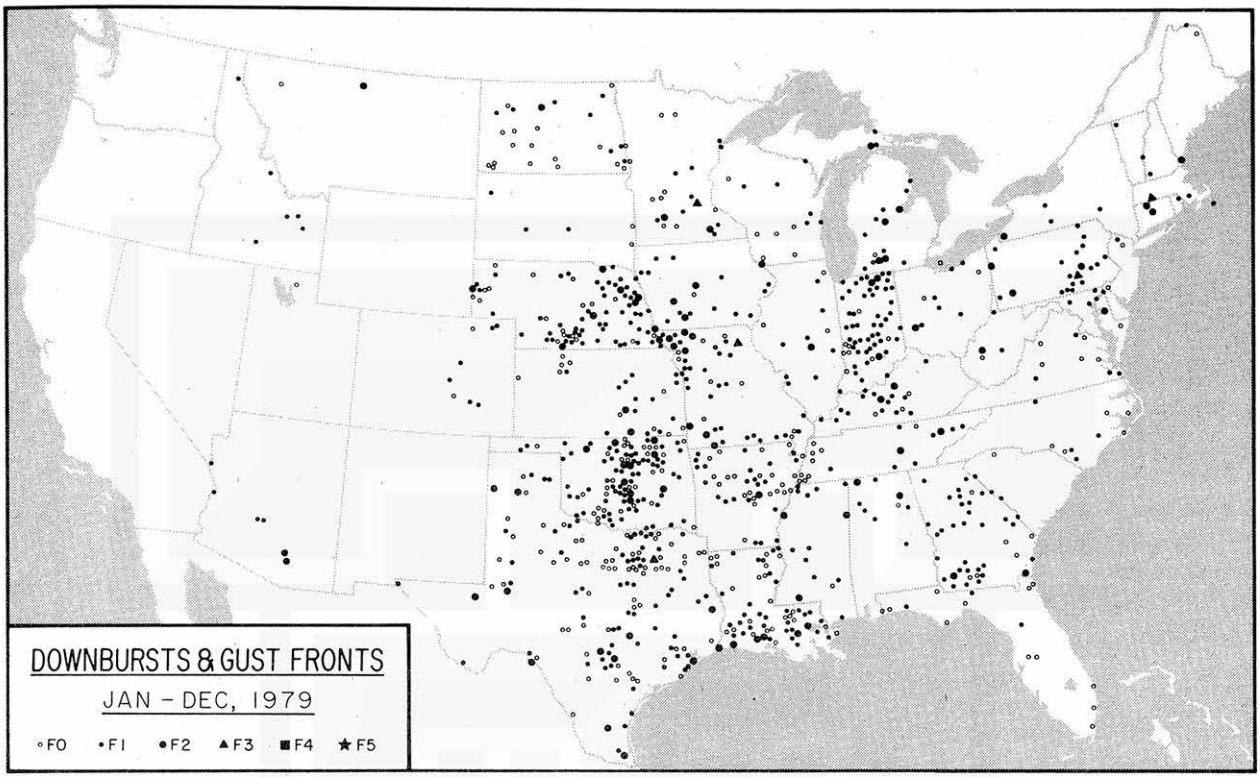

FIG. 6. Distribution of non-tornadic damage in 1979 coded with F scale. NOAA's *Storm Data* were used as the exclusive data source. Note that large frequencies were reported from Indiana, Nebraska and Oklahoma. Mapped by Neil Levine.

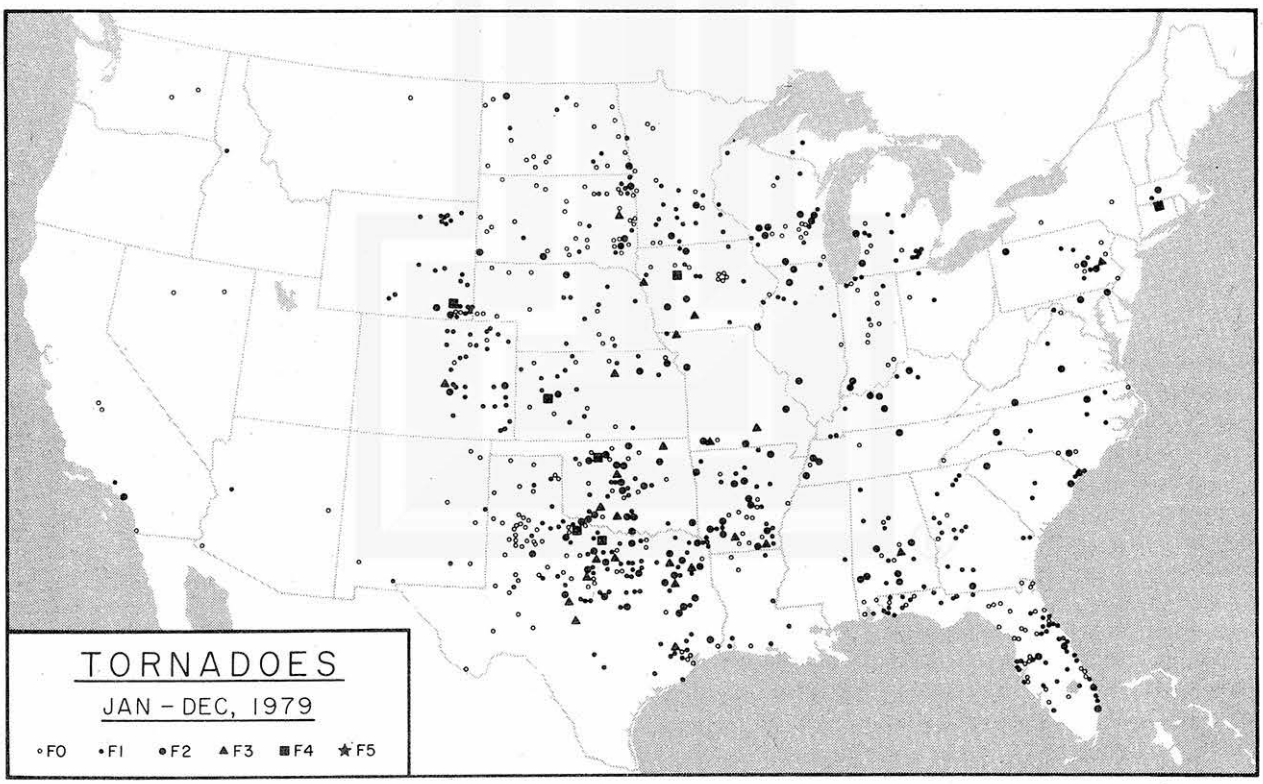

FIG. 7. Distribution of tornadoes in 1979 coded with F scale. Large frequencies were reported from South Dakota, Wyoming, Colorado, Oklahoma, Texas, Arkansas and Florida. Based on DAPPL tornado tape, The University of Chicago.

TABLE 1. Proposed classifications of tornadoes in relation to wind speeds or losses in dollars. Based on a review by Abbey.[3]

Year	Author	Country	Wind-speed range	Scale	Rated tornadoes Number (years)
1890	Hazen	U.S.A.	in dollars	1, 2, 3	2221 (1873–88)
1945	Seelye	New Zealand	not specified	0, 3, 5	162 (1919–44)
1971	Fujita	U.S.A.	18–142 m s^{-1}	0 to 5	25 825 (1916–79)
1975	Dames & Moore	U.S.A.	22–134 m s^{-1}	1 to 6	unknown (unknown)
1976	Meaden	England	19–151 m s^{-1}	1 to 11	unknown (unknown)

A-E-I-O-U scale is subdivided into α (larger) and β (smaller) scales.

3. Tornadoes and high winds

Severe thunderstorms often induce damaging winds grossly divided into tornado and straight-line wind. Aerial photographic surveys of damage areas in recent years have revealed, however, that there exists a third type of damaging wind identified as downburst. The characteristics of these damaging winds are as follows:

- Tornado: highly convergent swirling wind affecting a relatively narrow path.
- Straight-line wind: nondivergent, straight-line winds of damage-causing intensity seen just behind an advancing gust front.
- Downburst: highly divergent, straight or curved winds of damage-causing intensity.

Tornado data have been collected systematically since 1916, confirming over 26 000 storms as of 1980. Since 1959 all tornadoes, confirmed officially, are listed in NOAA's *Storm Data* published monthly.

Frequencies of non-tornadic winds have not been recorded systematically. NOAA's *Storm Data*, however, include a large number of high-wind incidents associated with thunderstorms. Fig. 6 shows the distribution of these non-tornadic winds (mostly downbursts and gust fronts) included in the 1979 *Storm Data*. The total number of incidents was 798 which is 2% more than 779, the total number of tornadoes in the same year (Fig. 7).

A comparison of Figs. 6 and 7 reveals convincingly that there are significant, state-by-state variations in the reported numbers of these two types of storms. These variations are (i) Georgia, Indiana, Louisiana and Nebraska reported significantly more high winds than tornadoes; (ii) Colorado, Florida, South Dakota and Wyoming reported significantly more tornadoes than high winds; and (iii) combined frequencies of tornadoes and high winds appear to be low in Illinois, Kansas and Mississippi and high in Oklahoma. These variations may or may not represent the true incidents of tornadoes and high winds in the year 1979, because possible differences in the storm-identification methods and practice adopted by each state in 1979 may as well contribute to the variations in (i), (ii) and (iii). Similar statistics in the years prior to 1979 are now being made in an attempt to determine their long-term variations.

Tornado is defined in the *Glossary of Meteorology* (1959) as "a violently rotating column of air, pendant from a cumulonimbus cloud, and nearly always visible as a funnel cloud." Nonetheless, some tornadoes are hidden in blinding rain or in the dark, necessitating their confirmation exclusively on the basis of damage characteristics determined by post-storm surveys.

One can easily determine the paths of violent tornadoes which smash and debark trees in forest, evacuate debris and erode soil in open fields, or blow down even low grasses. Paths of weak tornadoes are often lost in the open field or in the grass land, giving an impression of successive touchdowns on weak structures such as mobile homes and outbuildings. As a matter of fact, we cannot always distinguish weak tornadoes from downbursts or straight-line winds based on ground survey alone.

a. Tornado scales

There have been five schemes of classifying tornadoes on the basis of either wind speed or loss in dollars. Table 1 was prepared by summarizing an extensive review by Abbey.[3] Hazen (1890) utilized a scale of classes 1, 2 and 3 which are determined by the average loss in dollars. Seelye (1945) classified New Zealand tornadoes into Class 0 (funnel cloud with no or slight surface disturbance), Class 3 (outbuildings, verandas and roofs carried away) and Class 5 (well-constructed buildings demolished). A system of classifying tornadoes was proposed by Dames & Moore to the Nuclear Regulatory Commission in an unpublished document. The scheme relates structural damage with overlapping wind speeds.

The TORRO tornado scale was developed in England by Meaden (1976). The wind speed corresponding to the TORRO scale T is computed from

[3] Abbey, R. F. Jr., 1976: Risk probabilities associated with tornado wind speeds. *Proc. Symposium on Tornadoes*, Texas Tech University, 177–236. [Institute of Disaster Research, Texas Tech University, Lubbock 79409].

$$V_T = 2.36(T + 4)^{1.5}, \quad (1)$$

where V_T denotes the T-scale wind speed (m s^{-1}). The mean increment of the wind speed per scale is 12 m s^{-1} (27 mph).

The Fujita-scale (F-scale) wind speed was designed to connect smoothly the Beaufort force 12 with Mach number 1 in 12 steps. The mean increment of the wind speed per scale is 21 m s^{-1} (46 mph). F-scale wind speeds are computed from

$$V_F = 6.30(F + 2)^{1.5}, \quad (2)$$

where V_F denotes the F-scale wind speed (m s^{-1}).

The initial specifications of F-scale damage were devised in 1971 by Fujita,[4] leading to the experimental classification of U.S. tornadoes during the 1971 tornado season. Meanwhile, Fujita *et al.* (1972) applied the classification scheme to Japanese tornadoes. Fujita (1973) also attempted to assess tornadoes around the world with the F scale.

In 1973, National Weather Service Offices in the contiguous United States began assessing tornado F scales for their inclusion in two tornado tapes:

NSSFC (National Severe Storms Forecast Center) tornado tape produced and being updated at NSSFC, Kansas City, Missouri. This tape includes F scale, path length, longitudes and latitudes of touchdown and liftoff points, state, county, deaths, injuries, time, date, etc.

DAPPL (Damage Area Per Path Length) tornado tape produced and being updated at The University of Chicago, Chicago, Illinois. This tape includes F scale, path lengths in 15 min × 15 min sub-boxes of longitudes and latitudes, deaths, injuries, time, date, etc.

As of the end of 1980, more than 26 000 tornadoes were assessed with F scale on the basis of the following damage specifications along with the reference damage photographs in Fig. 8.

b. F-scale damage specifications

(F0) 18–32 m s^{-1} (40–72 mph): Light damage
Some damage to chimneys; break branches off trees; push over shallow-rooted trees; damage sign boards.

(F1) 33–49 m s^{-1} (73–112 mph): Moderate damage
The lower limit (73 mph) is the beginning of hurricane wind speed; peel surface off roofs; mobile homes pushed off foundations or overturned; moving autos pushed off the roads.

(F2) 50–69 m s^{-1} (113–157 mph): Considerable damage
Roofs torn off frame houses; mobile homes

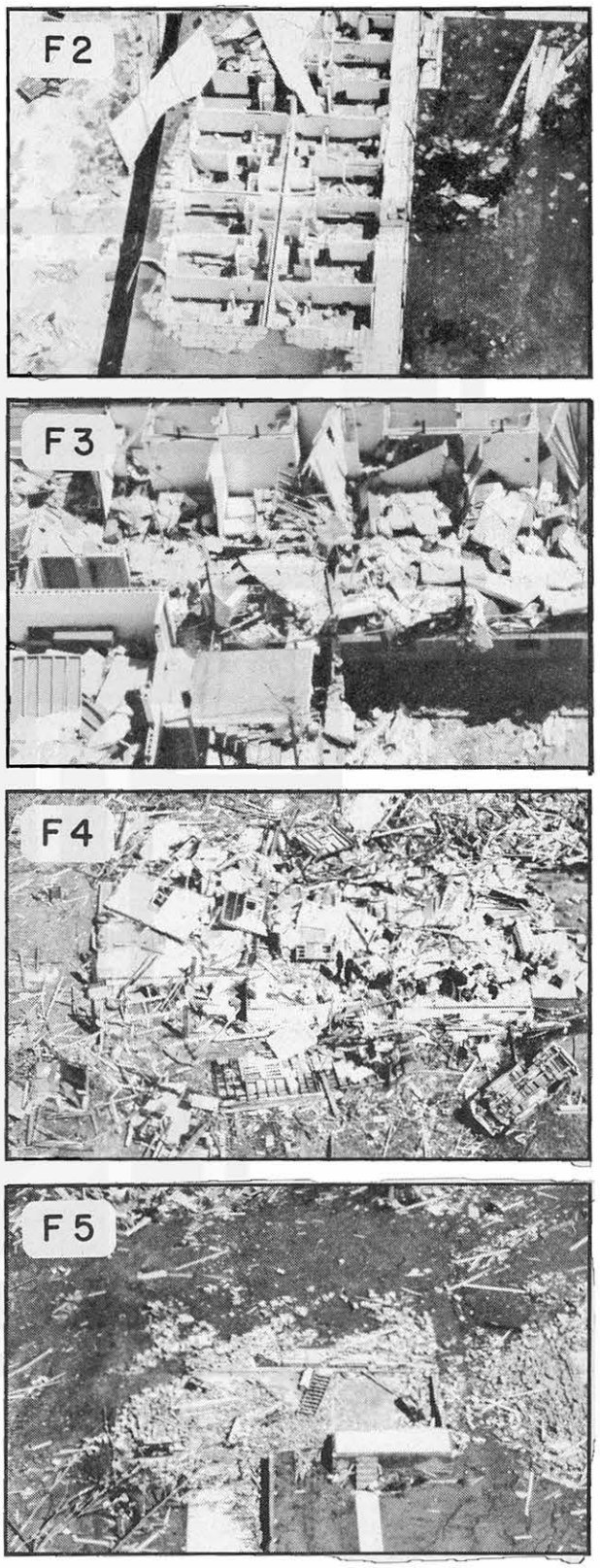

FIG. 8. Reference photographs of F2–F5 damage, which correspond to the F-scale damage specifications being used in rating U.S. tornadoes for producing and updating NSSFC and DAPPL tornado tapes.

[4] Fujita, T. T., 1971: Proposed characterization of tornadoes and hurricanes by area and intensity. SMRP Res. Pap. 91, University of Chicago, 42 pp.

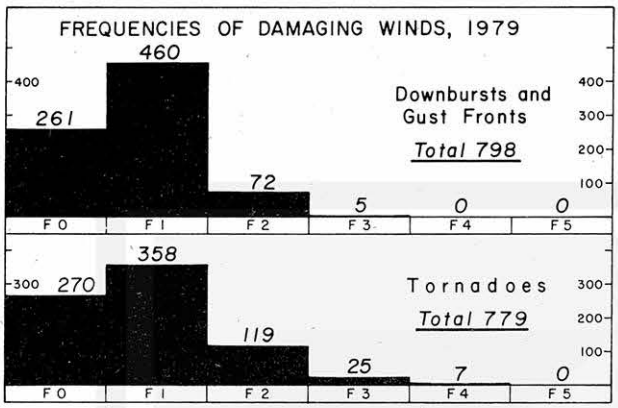

FIG. 9. F-scale distribution of tornadoes and thunderstorm-induced high winds in 1979. 91% of high winds were rated as F0 and F1 storms.

demolished; boxcars pushed over; large trees snapped or uprooted; light-object missiles generated.

(F3) 70–92 m s^{-1} (158–206 mph): Severe damage
Roofs and some walls torn off well-constructed houses; trains overturned; most trees in forest uprooted; heavy cars lifted off ground and thrown.

(F4) 93–116 m s^{-1} (207–260 mph): Devastating damage
Well-constructed houses leveled; structure with weak foundation blown off some distance; cars thrown and large missiles generated.

(F5) 117–142 m s^{-1} (261–318 mph): Incredible damage
Strong frame houses lifted off foundations and carried considerable distance to disintegrate; automobile-sized missiles fly through the air in excess of 100 m; trees debarked; incredible phenomena will occur.

(F6–F12) 142 m s^{-1} to Mach 1, the speed of sound
The maximum wind speeds of tornadoes are not expected to reach the F6 wind speeds.

The lack of the recorded wind speed in tornadoes in excess of 67.5 m s^{-1} (151 mph) which was reported by Fujita *et al.* (1970) does not permit us to calibrate F3 or worse damage against measured wind speeds. Damage specifications currently in use are approximate and are subject to revision when measurements of F3 to F5 wind speeds become available in the future years. The F-scale damage specifications outlined above has been kept unchanged since 1971, in order to avoid possible year-to-year variations of the assessment standard.

TABLE 2. F-scale breakdown of U.S. tornadoes during the 64 years, 1916–79. Based on the DAPPL (Damage Area Per Path Length) computer tape, The University of Chicago.

Year	F0	F1	F2	F3	F4	F5	Total
1916–79	6052	9037	7233	2696	680	127	25 825
	(23)	(35)	(28)	(10)	(2.6)	(0.5)	(100%)
1979 only	270	358	119	25	7	0	779
	(35)	(46)	(15)	(3.2)	(0.9)	(0.0)	(100%)

c. *Tornado F scale*

F-scale damage in the wake of a tornado varies along its path as well as in the direction perpendicular to the path. The F-scale ratings of tornadoes in NSSFC and DAPPL tapes are made by assigning the maximum F-scale damage inside the area affected by each tornado.

The relationship between Richter scale earthquake magnitudes and Mercalli scale earthquake intensities is similar in concept, but not in energetics, to that between tornado F scale and F-scale damage in the tornado. The former give the rating of the maximum energy released or the maximum wind speed induced, while the latter, the intensity of crustal or atmospheric movement in disturbances.

F-scale tornadoes, such as mapped in Fig. 7, are

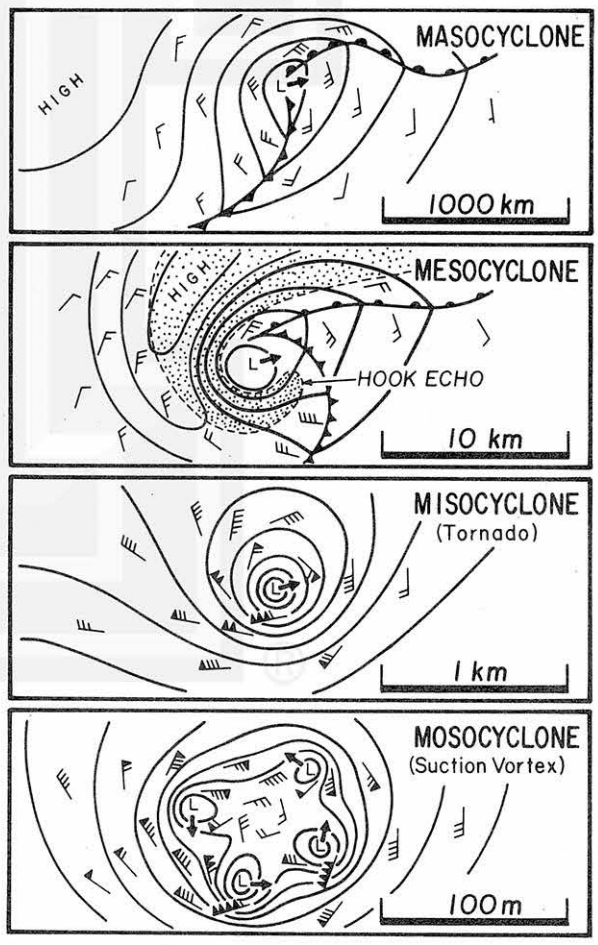

FIG. 10. Schematic drawings showing the features of maso-, meso-, miso- and mosocyclones.

identified with six terms: (F0) *Gale tornado*, (F1) *Moderate tornado*, (F2) *Significant tornado*, (F3) *Severe tornado*, (F4) *Devastating tornado*, and (F5) *Incredible tornado*. These are subgrouped into three categories—(F0 + F1) *Weak tornado*, (F2 + F3) *Strong tornado* and (F4 + F5) *Violent tornado*. Because F6 or stronger tornadoes are not expected to occur on the earth, they will be called *Inconceivable tornadoes* should they ever occur.

The 779 tornadoes in 1979 shown in Fig. 9 are rated by the tornado F scale described earlier. The year 1979 was a relatively inactive year of tornadoes; 81% were F0 and F1 and only 0.9% were rated as F4, the highest rating of the year (Table 2).

The high-wind events in Figs. 6 and 9 were rated and coded with the F scale. Of these, 261 (33%) were F0, 460 (58%) F1, 72 (9%) F2 and 5 (0.6%) F3, the highest rating. These results imply that a large number of tornadoes and nontornadic winds are either F0 or F1 (<50 m s^{-1}), making their distinction sometimes very difficult.

In support of both storm-type identifications and damage assessments, the author organized an aerial photographic survey team in 1967. Since then the areas of more than 350 tornadoes and 100 downbursts were flown over for taking photos from 300 to 1000 m above the ground. Sub-mesoscale patterns of airflow presented in this paper were depicted, mapped and confirmed based on these aerial photographs.

4. In search of sub-mesoscale cyclonic winds

A sequence of cyclones in Fig. 1 includes four scales of natural disturbances, cyclone (A scale), mesocyclone (E scale), tornado (I scale), and suction vortex (O scale). These cyclones are interrelated; an A-scale cyclone provides the spawning ground of an E-scale cyclone; E-scale cyclone provides that of I scale cyclone; and so on. It is of great interest to perform numerical/physical modeling of these cascading-scale cyclones (Fig. 10).

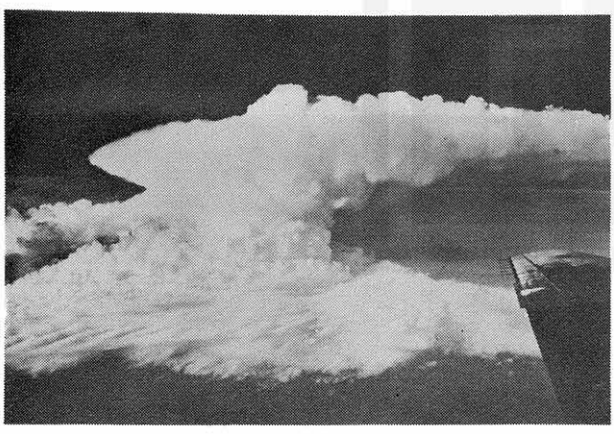

FIG. 11. Aerial view of a mesocyclone cloud, also called supercell, rotating thunderstorm and hook-echo storm. From U.S. Weather Bureau's DC-6 at 6000 m during the NSSP research flight on 21 April 1961. For further information, refer to Fujita (1963).

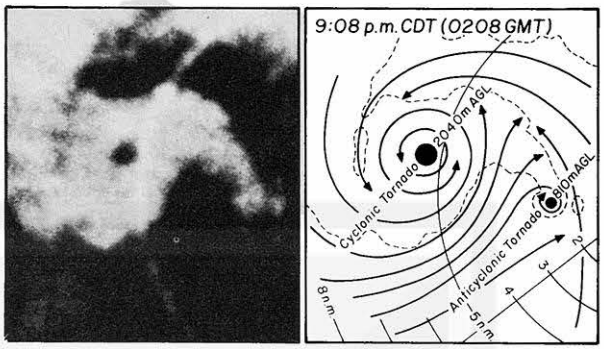

FIG. 12. WSR-57 radar picture of cyclonic and anticyclonic tornadoes to the northwest of Grand Island, Nebraska on 3 June 1980. Radar photo by the National Weather Service, Grand Island.

a. Mesocyclone

A tornado-producing mesocyclone, often called supercell, is a rotating thunderstorm with rotating updrafts and expanding anvil cloud (Fig. 11). The hook echo, a typical radar signature of the mesocyclone, was first detected by Stout and Huff (1953). Since then, the frequency of observations of hook echoes has increased significantly so that they have been used for tornado warnings. The effective warning of the Topeka, Kansas tornado by Garrett and Rockney (1962) is an excellent example.

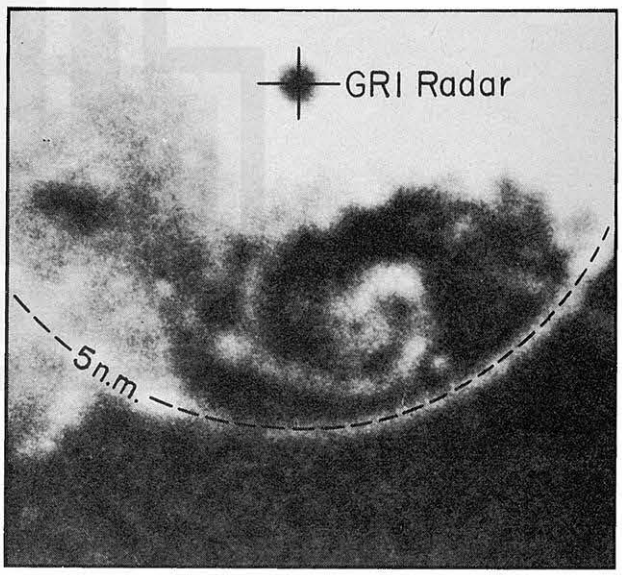

FIG. 13. WSR-57 radar picture of the Fifth Grand Island tornado at 2216 on 3 June 1980. The tornado was located near the inner end of a misoscale spiral echo. Radar photo by the National Weather Service, Grand Island.

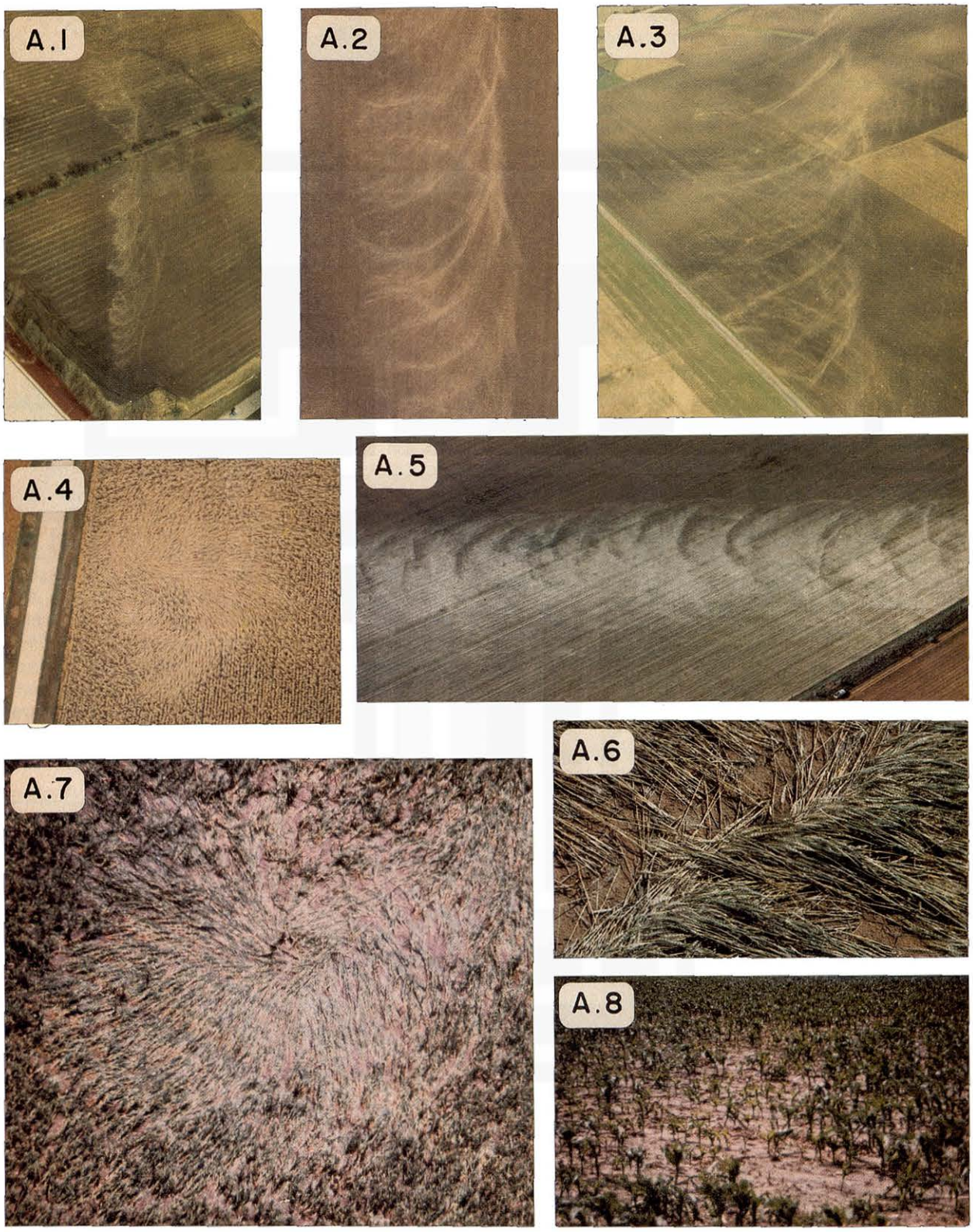

FIG. 14. Examples of ground marks left behind by suction vortices embedded inside tornadoes. Locations and dates of occurrences are: (A.1) Decatur, Illinois tornado 3 April 1974; (A.2) Magnet, Nebraska tornado, 6 May 1975; (A.3) Homer Lake, Indiana tornado, 3 April 1974; (A.4) Dubuque, Iowa tornado, 28 September 1972; (A.5) and (A.6) Pearsall, Texas tornado, 15 April 1973; (A.7) Mattoon Lake, Illinois tornado, 21 August 1977; (A.8) Grand Island, Nebraska tornado, 3 June 1980.

Single-Doppler detection of a mesocyclone by Brown *et al.* (1971) at the National Severe Storms Laboratory, Norman, Oklahoma signaled the beginning of the real-time use of Doppler radars for detecting mesocyclones. To meet the requirement of simultaneous presentation of single-Doppler data, a multimoment Doppler display system was developed by Burgess *et al.* (1976), for use in early detection of mesocyclones with a 30 min average lead-time before tornadoes.

Dual- and multiple-Doppler radars are operated for collecting reflectivity and velocity data in determining three-dimensional velocities inside mesocyclones. Three-dimensional velocity patterns in various modes of presentation were reported by Ray (1976), Brandes (1978), Ray *et al.* (1980) and many others.

The smallest mesocyclone depicted with triple-Doppler analysis was reported by Carbone and Serafin[5] and also by Wilson *et al.* (1980). The triple-Doppler analysis with a 300 m grid spacing depicted the circulation field extending only 4–5 km across.

b. *Misocyclone (tornado)*

By definition of scale, the wind field of misocyclones is 40–4000 m in horizontal dimension. Most tornadoes, with exceptions of very small ones, are fast-rotating misocyclones.

A long-distance scanning by non-Doppler radar usually fails to identify misocyclone echoes because they are too small to be depicted and identified. At a close range, however, a misocyclone can be seen as an echo-free eye (Fig. 12) at the inner end of a misoscale spiral (Fig. 13) or other signatures such as a diffused blob of echo.

Fig. 12 is particularly interesting, because it shows a pair of cyclonic and anticyclonic tornadoes within the 9.6 km (5.2 n mi) range of the Grand Island, Nebraska radar. Simultaneous observations of cyclonic and anticyclonic tornadoes, as reported by Fujita (1977) and Brown and Knupp (1980), do not appear to be as rare as had been suspected. Misoscale modelers should be attracted by such a pair of cyclonic and anticyclonic tornadoes which were evidenced in the Grand Island storm on 3 June 1980 and in the central Iowa storm on 13 June 1977.

c. *Mosocyclone (suction vortex)*

The horizontal dimensions of mosocyclones extend between 40 cm and 40 m by the definition of the scale. Most of the suction vortices in tornadoes are included in this scale which is four orders of magnitude smaller than mesoscale. In search of wind traces of mosocyclones in tornadoes, the University of Chicago's survey team attempted various types of aircraft maneuvers at low levels. In most cases the traces of high winds can be seen best from one specific direction relative to the sun. Flight altitudes must be determined accordingly.

Fig. 14 shows the trace of mosocyclones (suction vortices) selected from the collection of aerial photographs taken since 1967. These pictures reveal the fact that some suction vortices (A.4) and (A.7) swirled without traveling, while others orbited

[5] Carbone, R., and R. Serafin, 1980: A severe winter squall line, Part II: Kinematic structure deduced from Triple Doppler radar observations. *Preprints 19th Conf. Radar Meteorology*, Miami Beach, Amer. Meteor. Soc., 9–16.

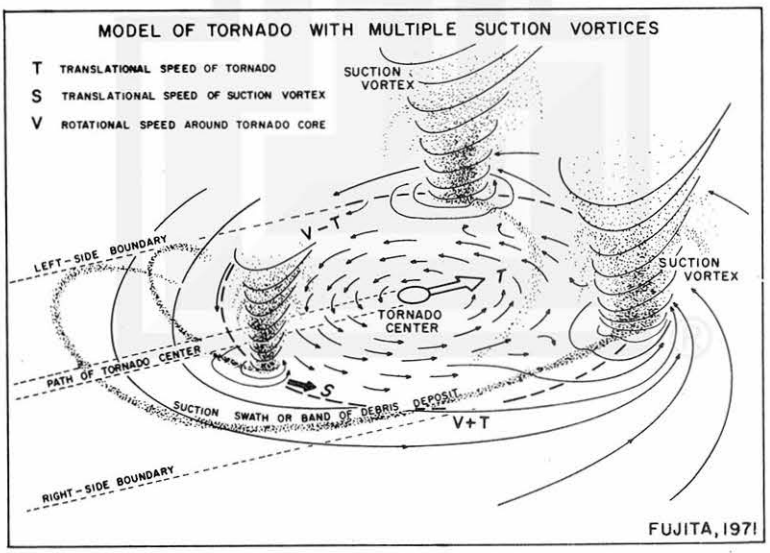

FIG. 15. A model of a tornado with multiple suction vortices proposed by the author in 1971.

FIG. 16. Swath of an orbiting suction vortex in the Birmingham tornado on 4 April 1977. The width of the F4 wind is estimated to be only 3–5 m wide, extending across the center of the picture. Trees in the swath were debarked and flattened, converging toward the swath center.

around the center of the parent tornado which traveled across the open field.

d. Orbiting suction vortices

Aerial photographs of circular ground marks left behind the Scottsbluff tornado were first discussed by Van Tassel (1955), leading to the 216 m/s^{-1} (F8) windspeed estimated under the assumption of a single object rotated inside the funnel cloud on the ground of sandy soil.

Numerous aerial photographs of circular and cycloidal ground marks obtained since then imply, however, that the marks were produced by three to five suction vortices which orbited simultaneously around the core of the parent tornado. A schematic view of such a tornado with multiple suction vortices was made by Fujita[1] (Fig. 15). An existence of multiple vortices reduces the estimated wind speed based on ground marks in the wake of tornadoes.

After an extensive aerial survey of the Palm Sunday tornadoes in April 1965, Fujita *et al.* (1970) devised a method of computing the orbital speed of suction vortices (then called suction spots) based on the geometric shape of the cycloidal orbital paths, including the loop widths and orbit radii. The orbital speeds inside one of the Palm Sunday tornadoes (rated F4) were 46–53 m s^{-1} while the parent tornado was traveling at 28 m s^{-1}. The maximum traveling speeds of suction vortices while on the right side of the tornado turned out to be 74–81 m s^{-1}.

Using the identical method of computation, Agee *et al.* (1977) obtained orbital speeds inside the Lafayette, Indiana tornado (rated F4) of 44–61 m s^{-1}. An addition of 22 m s^{-1}, the traveling speed of the parent tornado, results in the maximum traveling speeds of suction vortices, 66–83 m s^{-1}.

The wind speed in the direct path of a suction vortex is the sum of its traveling and spinning velocities. Ground marks can be used in estimating the translational speed of the vortex, but not the spinning motion. Forbes[6], through photogrammetric analysis of motion pictures, obtained a 39 m s^{-1} mean spinning rate of one of the suction vortices in the Parker, Indiana tornado of 3 April 1974. The fact that suction vortices are often accompanied by their own individual funnel clouds implies that a 20–30 m s^{-1} spinning rate may be conservative.

By adding the spinning motion estimated above, to the translational speed, the maximum wind speeds along the narrow swaths in the Palm Sunday tornado discussed above are 94–111 m s^{-1} and those in the Lafayette tornado, 86–113 m s^{-1}. These values fall within the range of their rated F4 windspeeds (93–116 m s^{-1}).

The width of F4 winds, most likely to occur only inside the orbiting suction vortices, are expected to be very narrow. Fig. 16 shows an aerial photograph

[6] Forbes, G. S., 1978: Three scales of motion associated with tornadoes. NUREG/CR-0363. 359 pp. [U.S. Nuclear Regulatory Commission, 7915 Eastern Ave., Silver Spring, Md. 20910].

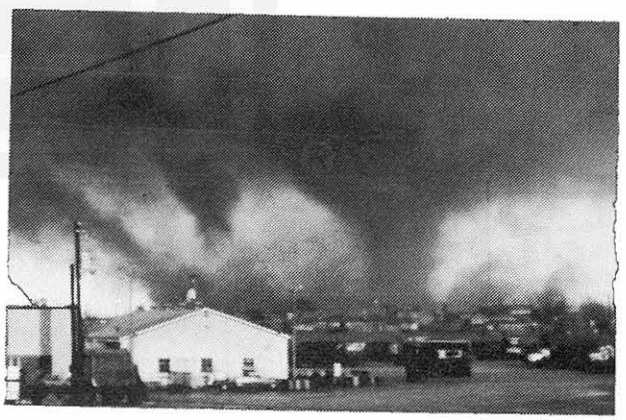

FIG. 17. Six suction vortices in various stages of development. Courtesy of Mr. Floyd Styles, Wichita Falls, Texas.

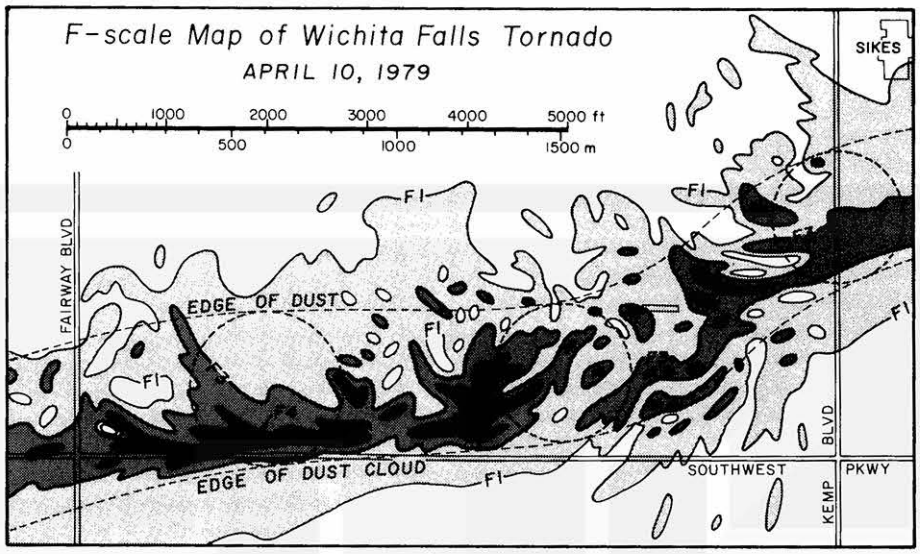

FIG. 18. F-scale contours in the south section of Wichita Falls. The size and location of the swirling column of dust and debris are shown with dashed circles.

of an F4 swath, only 3–5 m wide. Two houses inside the swath disappeared while trees, debris and cars were pointing toward the direction of devastating suction-vortex winds.

Six suction vortices in various stages of development are seen in one of the photographs taken by Floyd Styles when the 10 April 1979 tornado was to the east of Wichita Falls, Texas (Fig. 17). The same tornado, while traveling over the city, was a huge swirling column of dust, 400–500 m in diameter. In spite of the fact that no suction vortex was visible through the thick dust cloud over the city, F-scale contours in Fig. 18 clearly suggest the existence of one or more suction vortices hidden inside the swirling cloud. Some lucky houses inside the dust column escaped with less than F1 damage, losing only a few roof tiles.

Aerial and ground photographs of suction-vortex marks often suggest the width of the extreme wind to be less than 1–2 m. Fig. 14 (A.6) shows the twisted wheat inside one of the suction vortex mark in (A.5). Young corn stalks in (A.8) had been pulled out of the clayey ground along a crescent-shaped curve in which the bare ground is only 30 cm wide.

The maximum wind speed of tornadoes have been estimated by various means, such as photogrammetry, engineering, minimum pressure, funnel shape, etc. The basic question still left unanswered is: "How can we measure accurately the short-lived maximum wind speeds inside mosocyclones?" Session 7 of the Symposium on Tornadoes at Texas Tech University, chaired by Kessler,[7] included the presentation and discussion of the maximum tornado wind speeds. One of the clarification questions was related to the scale, both in time and space, of the extreme winds. Square centimeter, square meter, or square dekameter in space and millisecond, second or minute in time are the resolutions in estimating the uppermost wind speed inside tornadoes.

The scale of suction vortices (mosocyclone) in tornadoes strongly suggests that the extreme winds in a tornado are often <1–2 m wide. However, an object in the wind does not always respond to the maximum wind, because a small-scale airflow is distorted by a larger scale object.

Numerical modeling of suction vortices is important in estimating rapidly changing pressure and wind fields which cause severe damage in large tornadoes. In spite of anticipated difficulties in modeling mososcale vortices, Rotunno's (1979) axisymmetric calculations of tornado-like vortices have been extended by him into three-dimensional calculations, obtaining the fields of two suction vortices orbiting around the core of the parent tornado. The result clearly shows that the extreme winds within the misocyclone (tornado) are concentrated inside the mosocyclones (suction vortices) which orbit around the center of their parent cyclone.

e. Twin suction vortices

Vortex marks of a small tornado in Fig. 14 (A.1) were weakened by a line of trees and disappeared at the tree crossing. After the crossing, the marks reappeared while the core diameter of the parent tornado gradually increased. A medium-size tornado

[7] Kessler, E., 1976: Recent developments in tornado research. *Proc. Symposium on Tornadoes*, Texas Tech. Univ., 431–435, 437–443, 673–677. [Institute of Disaster Research, Texas Tech Univ., Lubbock, Texas 79409].

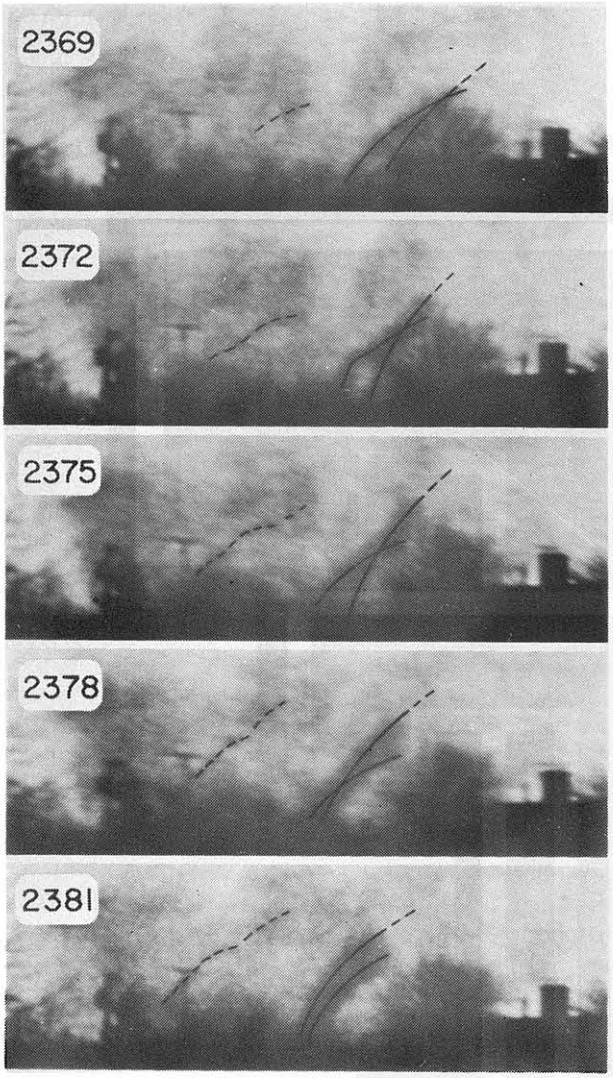

FIG. 19. Twin suction vortices which were twisting around each other inside the Xenia tornado of 3 April 1974. Enlargements of every third frame of the tornado movie taken at 18 frames s^{-1}. Courtesy of Mr. Bruce Boyd.

often leaves behind a number of cycloidal marks, regularly spaced and relatively smooth in appearance.

Cycloidal marks in the wake of a medium-size tornado (A.2) are relatively smooth and regular. Although some of these marks do not represent complete cycloidal curves, they are produced by several suction vortices which orbit around the tornado center with fluctuating intensities.

Cycloidal marks of large-core tornadoes sometimes show "double tracks", suspected to be produced by twin suction vortices (A.3). At one point, these double tracks cross each other implying that twin vortices rotate around each other as they orbit around the center of the parent tornado.

The existence of twin vortices was confirmed in the Xenia tornado movie taken by Bruce Boyd. Five frames enlarged from his movie show a pair of twin vortices which moved from right to left twisting around each other (Fig. 19). The evidence of the twin suction vortices in Figs. 14 (A.3) and 19 are the smallest scale vortices which were confirmed based on aerial photographs and tornado movies currently available to the author.

f. Stationary suction vortices

Apparently, some suction vortices form suddenly inside tornadoes and disappear within a short time. These vortices leave behind the swirl mark with a calm eye near the center of the swirl.

Fig. 14 (A.4) shows a swirl mark with an eye of weak wind surrounded by strong cyclonic winds which flattened cornstalks. It is suspected that the swirling winds were transient, lasting less than one minute. Another example (A.7) is characterized by a large crossing angle (70–80°) of the inflow around the 20–30 m radius of the vortex. The eye of the vortex, 8–10 m in diameter, was disturbed slightly when the vortex moved toward the upper right. This vortex mark is one of the 20–25 marks found one after another in the wake of the Mattoon Lake, Illinois tornado of 21 August 1977.

5. In search of sub-mesoscale high winds

A sequence of high-pressure systems in Fig. 1 includes masohigh (regular anticyclone), mesohigh (pressure dome) and misohigh (pressure nose). Characteristic scales of motion of these high-pressure disturbances are presented schematically in Fig. 20, although a possible high pressure accompanied by the burst swath has not been confirmed.

The report of the Thunderstorm Project by Byers and Braham (1949) distinguishes the "pressure dome" from the "pressure nose". The pressure dome, later called mesohigh by Fujita *et al.* (1956), is a dome of cold air produced by a group or a line of thunderstorms. The pressure nose in the Thunderstorm Project Ohio Network (3 km station separation) was detected by only one station at any given time, indicating that the maximum diameter of the nose was <6 km.

A succession of subscale highs in Fig. 20 are characterized by their own time scale. A masohigh may last for days and weeks and a mesohigh, only 3–18 h. The life of a misohigh will be no more than 15–20 min before it expands into a small mesohigh.

An extensive aerial photography of the effect of diverging winds was performed in 1977 through 1980, thus identifying sub-mesoscale outflows of damaging winds. These outflows defined in the Appendix at the end of this paper are as follows:

- Downburst, accompanied by either a small mesohigh or a large misohigh.

• Microburst, misoscale downburst accompanied by a large misohigh.
• Burst swath, likely to be accompanied by a small miso- or mosohigh that has not been confirmed.

Initially, we made extensive low-level flights over the areas swept by gust fronts and pressure-jump lines accompanied by the reported 27 m s^{-1} (60 mph) × wind speeds. Against our expectations, the damage by straight-line winds behind these gust fronts turned out to be minimal. Isolated tree falls, broken branches, and other types of damage rated F0 or F1 were all we could find there.

The horizontal dimensions of the significant damage visible from a low-flying Cessna were almost always meso-β (4–40 km) scale or smaller, which is the scale of the pressure nose.

Fig. 21 shows typical views of wind damage selected from numerous color photographs taken from 150 to 600 m above ground. Plate (B.1) shows the tree damage in one of the 25 downbursts in northern Wisconsin on 4 July 1977. Individual downbursts were 10–20 km across, characterized by the F1 to F2 damage.

Plate (B.2) presents a view of a corn field damaged by a microburst. The microburst cell, traveling from the top to the bottom of the picture, blew down corn crops and opened up a number of hay bundles with an estimated F1 wind. A significant pattern of misoscale divergence is visible in the picture.

Winds in a "burst swath" are highly localized. Its average width is only about 100 m. Damaged trees in (B.3) indicate that the width at touchdown was 40 m and that the airflow was highly divergent accompanied by a pair of cyclonic and anticyclonic circulations on both sides of the burst swath center line.

A long and narrow burst swath appears like a path of a tornado (B.4). However, a close-up view (B.5) reveals the flow inside a burst swath to be highly divergent. This is in contrast with a narrow swath of a tornado, in which the airflow inferred by damage is highly convergent. A tornado swath can always be distinguished from a burst swath by photographing the wind effects from a low-flying aircraft at a proper angle of view. However, their distinction based on ground inspection alone is often very difficult, if not impossible.

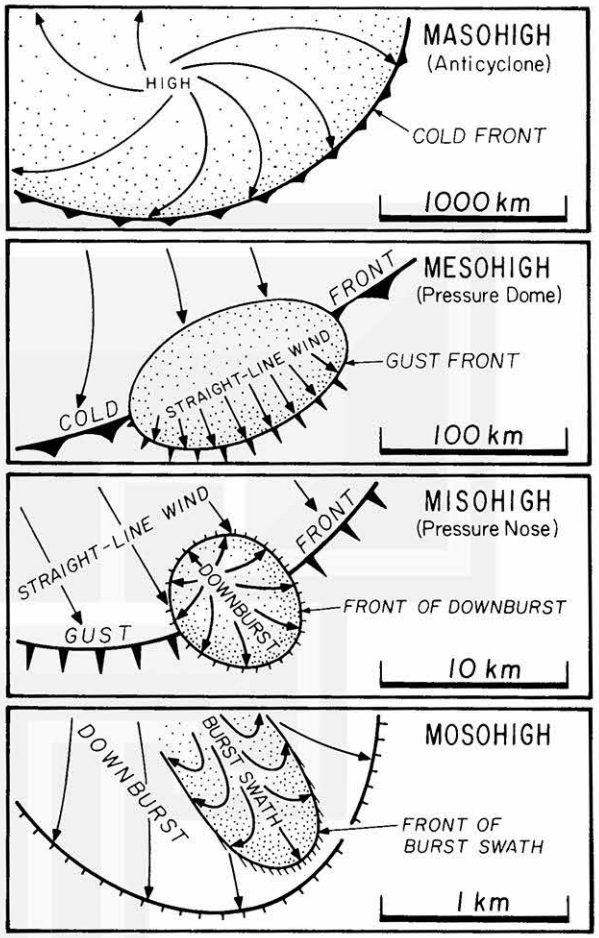

FIG. 20. Schematic drawings showing the airflow patterns accompanied by maso-, meso-, miso- and mosohigh (unconfirmed).

a. Downburst and bow echo

The "line echo wave pattern" by Nolen (1959) and the bulge or concave-shaped echo by Hamilton[8] have been known to be the inducers of squall-line-related high winds. Recently, Fujita[9] pointed out that hook and bow echoes are the inducers of mesoscale downbursts (4–20 km across). A hook echo, by virtue of its rotational motion, induces downbursts with twisting airflow, called the "twisting downburst". A bow echo, on the other hand, induces downbursts which burst out of the center of the bow.

During Project NIMROD (Northern Illinois Meteorological Research On Downburst), a fact-finding project of downbursts, bow-echo induced strong downbursts occurred on 25 June 1978. The downbursts left behind a 6 km wide swath of damaging winds rated F1. Two tornadoes, rated F1 and F2, occurred during the downburst. The stronger one, Tornado A (Fig. 22) which began at 1310 CDT traveled 8 km, killing one person.

This bow echo at 1301 CDT, when the downbursts in Fig. 22 had started, was displayed on the NCAR's Research Data Support System (RDSS) and pre-

[8] Hamilton, R. E., 1970: Use of detailed intensity radar data in mesoscale surface analysis of the July 4, 1969 storm in Ohio. *Preprints 14th Radar Meteorology Conf.*, Tucson, Amer. Meteor. Soc., 339–346.

[9] Fujita, T. T., 1978: Manual of downburst identification for Project NIMROD. SMRP Res. Pap. 156, University of Chicago.

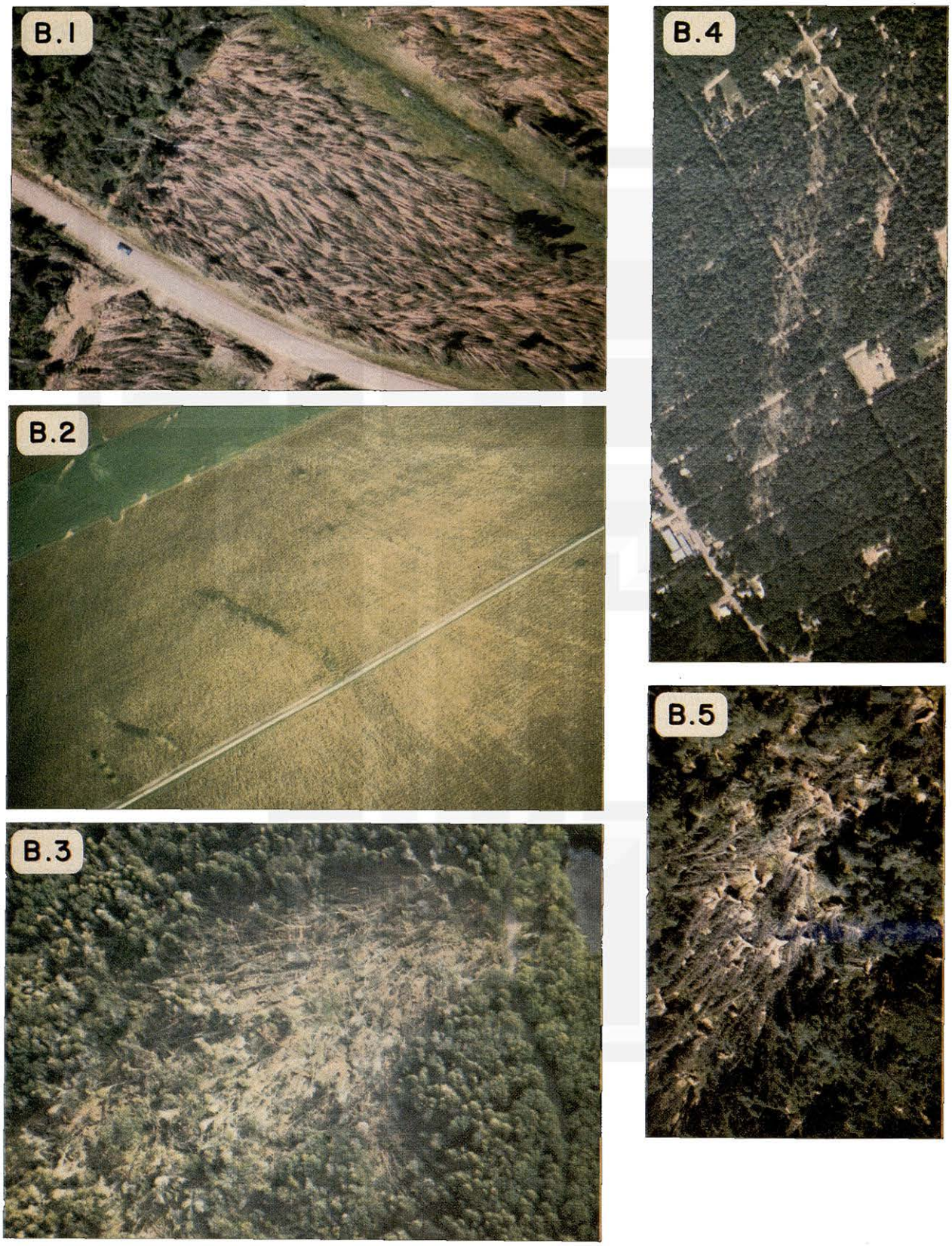

FIG. 21. Examples of wind effects of downbursts and burst swaths. Location and dates of occurrences are: (B.1) northern Wisconsin downburst, 4 July 1977; (B.2) Gessie, Indiana microburst, 30 September 1977; (B.3) Cornell, Wisconsin burst swath, 30 July 1977; (B.4) and (B.5) Northwood Beach, Wisconsin burst swath, 4 July 1977.

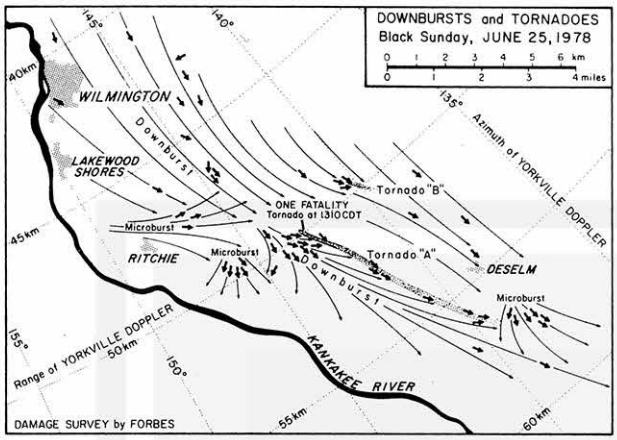

FIG. 22. Downbursts and tornadoes to the southeast of Wilmington, Illinois, near 50 km range and 140° azimuth of the Yorkville (YKV) Doppler radar. Damaging winds were on the ground between 1300 and 1320 CDT 25 June 1978. Damage survey by Greg Forbes during Project NIMROD, 1978.

sented by Wilson *et al.* (1980). A pair of color photos showing reflectivity and velocity fields reveals that a tongue of downburst winds was rushing out of a weak-echo channel in the bow echo.

The field of dual-Doppler velocities of the same bow echo, between 1321 and 1325 CDT several minutes after the end of the downbursts, is presented in Fig. 23. It is seen that high winds are still pushing out of the central region of the bow echo where the width of the 50 dBZ echo (shaded) is relatively narrow. Apparently, the weak-echo region near the center of a bow echo is where the downburst winds are expected to be the highest.

On the basis of both Doppler and non-Doppler analyses of a number of bow-echo-induced downbursts, Fujita[2] proposed a model of the evolution of a bow echo (Fig. 24). The initial stage of a bow echo is a tall thunderstorm with a gust front located along the leading edge of the activity line. This is Stage A. In Stage B, a downburst descends from the tall echo, distorting the line echo into a bow-shaped bulge. The downburst intensifies at the location of the arrow attached to a bow. When the downburst reaches its mature intensity, the bow echo takes the shape of a spearhead, accompanied frequently by a channel (or trench) of weak echo located along the center axis of the downburst flow. Downburst-induced tornadoes are likely to form in this stage.

As the downburst weakens, after pushing ahead of the parent bow echo, a mesoscale circulation dominates the area of the bow echo. Then a rotating head with an appearance of a hook echo forms near the center of the mesoscale circulation. The final stage of bow echo often turns into a comma-shaped echo which gradually disappears along with the weakening mesoscale circulation.

Fig. 25 presents radar pictures of a significant bow echo on 6 August 1977. The echo was bow-shaped at 1506 CDT. It turned into a spearhead echo at 1548 CDT when the downburst air was dashing out of the weak echo region of the spearhead. The peak intensity of the downburst at this stage was F2. At 1622 CDT the bow echo finally turned into a comma echo.

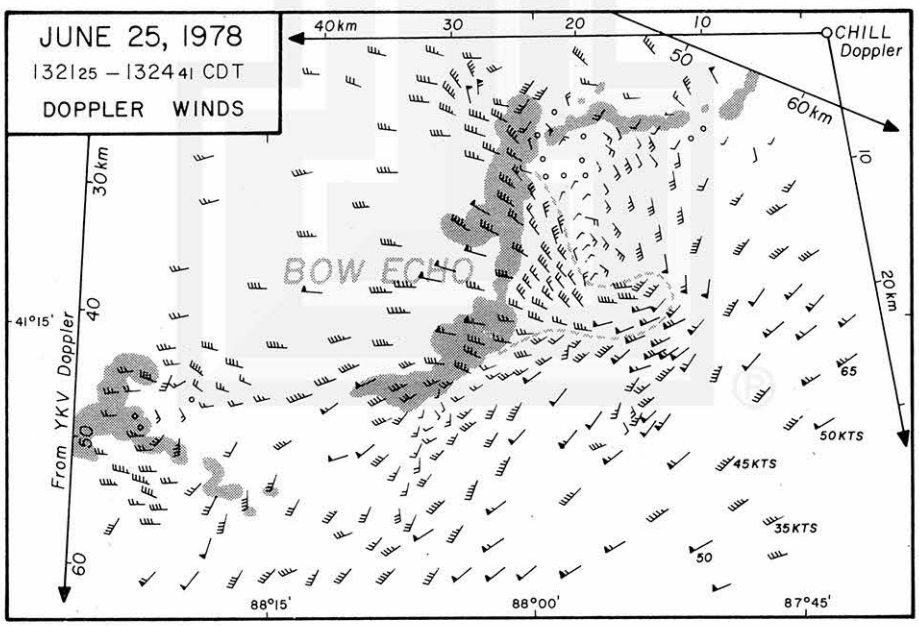

FIG. 23. Dual-Doppler winds on 3.5° scan surface of the YKV radar between 1321 and 1325 CDT 25 June 1978. Damaging winds mapped in Fig. 22 ended at 1320 at 58 km range and 135° azimuth of the YKV radar. The AGL height of the Doppler beam in the high-wind areas is 3.0–3.5 km.

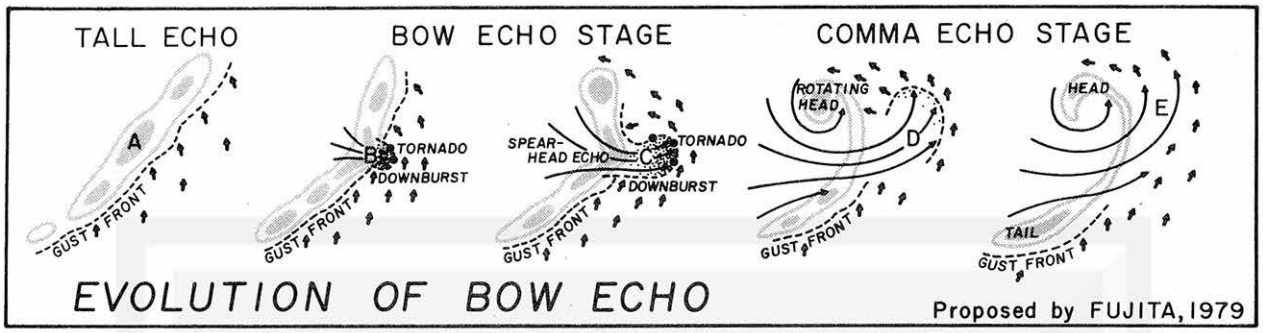

FIG. 24. Evolution of bow echo proposed by the author in 1979. In this model, a bow echo is produced by a downburst thunderstorm as the downflow cascades down to the ground. Finally, the horizontal flow of a weakening downburst induced a mesoscale circulation which distorts the initial line echo into a comma-shaped echo with a rotating head.

b. Microburst (misoscale downburst)

A microburst is a misoscale downburst with its horizontal dimension < 4 km. Fig. 26 shows a microburst photographed in Kansas on 1 July 1978. It is seen in the picture that the descending air spreads out violently on reaching near the ground.

A stationary microburst descends to the ground in its contact stage. As the cold air brought down by the microburst accumulates on the ground, a cushion of the cold air prevents the descending air from reaching the surface. As a result, the height of the extreme wind above the ground increases with time. Meanwhile, the intensity of the extreme wind decreases as the spreading depth increases (Fig. 27).

A traveling microburst, on the contrary, keeps descending in advance of the cold air which is left behind to form a mesoscale pressure dome. It is likely that the slanted surface of the cold air deflects the outburst winds forward (Fig. 28). A velocity cross section through the center of a traveling microburst was obtained on 29 May 1978 during Project NIMROD by using CP-3 Doppler radar (Fig. 29). This cross section shows ground-relative velocities computed by combining u and w component velocities. The extreme wind of the outburst flow is located ~1.5 km in advance of the downflow center. The burst front, located more than 1 km ahead of the maximum horizontal winds, was characterized by the rising current extending higher than 500 m above the ground.

The Doppler-measured height of the maximum wind, 32 m s^{-1}, was located only 50 m above the ground. The vertical wind shear beneath this maximum wind is as high as 0.6 s^{-1}. Above this height of the maximum horizontal wind, the windspeed of the outflow decreases gradually with altitude (Fig. 30).

6. Source height of downburst

Since Newton (1950), numerous studies suggested the need for the mid-level dry air for explaining thermodynamical properties of downdrafts in squall lines. On the other hand, a possibility of downdrafts initiating at the top of cumulus clouds was proposed by Squires (1958).

In explaining the fast-moving tongue of a spearhead echo which spawned downbursts at the JFK

FIG. 25. Radar pictures showing a bow echo which turns into a spearhead echo and then into a comma echo. During its spearhead stage, this bow echo produced a cluster of 10 downbursts near Springfield, Illinois, on 6 August 1977 (25 n mi range markers). Refer to Fujita.[9]

Airport, New York City, Fujita[10] and Fujita and Caracena (1977) speculated on the possibility of a long-distance descent of the cloud-top air, triggered by the collapsing phase of an overshooting top. The descending currents are assumed to entrain the environmental in-cloud air, because there is no means of bringing the undiluted cloud-top air of high potential temperature down to the ground.

In their recent paper, Lemon and Doswell (1979) proposed a mechanism of the rear-flank downdraft originating at near the jet stream level. The downdraft is assumed to be cooled by the evaporation of hydrometeors falling from the sloping echo overhang while the downward acceleration is provided by the vertical gradient of the non-hydrostatic pressure, similar to that proposed by Newton and Newton (1959).

Through triple-Doppler analysis of the Project NIMROD data, Heymsfield and Srivastava[11] depicted a downflow field extending from the cloud top at 8.4 km all the way to the ground. The downflow was located on the northwest side of a thunderstorm traveling northeast. At the cloud-top level there was a converging flow mainly from the northwest descending into the top of the downflow area, ~3 km across.

Emanuel (1981) attempted to explain downburst phenomena as penetrative downdrafts of the type discussed by Squires (1958), in which condensate is supplied to the unsaturated downdraft by turbulent mixing. This downdraft would originate in the middle-level dry air that has been entrained into the storm. There have been discussions both pro and con regarding the source height and the mechanism of downbursts. It will be necessary to make further attempts to find the mechanism by which some selected downdrafts descend to the ground to induce damaging winds in a misoscale area at a height of 50 m or even closer to the ground.

[10] T. T. Fujita, 1976: Spearhead echo and downburst near the approach end of a John F. Kennedy airport runway, New York City. SMRP Res. Pap. 137, University of Chicago. [This paper describes the JFK accident, introducing the term "downburst".]

[11] Heymsfield, G. M., and R. C. Srivastava, 1980: Doppler observation of the evolution of a thunderstorm. *Preprints 19th Conf. Radar Meteorology*, Miami Beach, Amer. Meteor. Soc., 342–349.

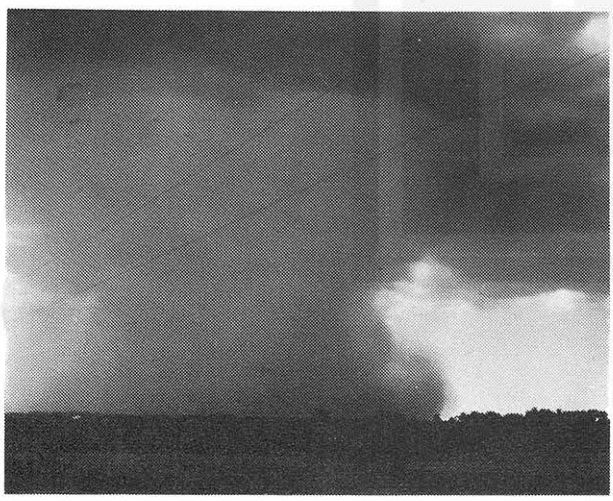

FIG. 26. A photograph of a microburst in action on 1 July 1978. Courtesy of Mr. Mike Smith.

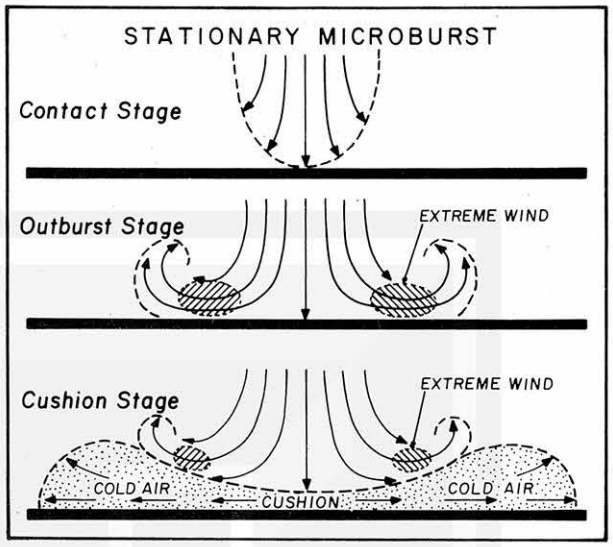

FIG. 27. Schematic diagram of a stationary microburst descending onto a cushion of cold air which weakens the outburst winds near the ground.

RHI cross section of microburst/downburst

During Project NIMROD, NCAR's CP-3 Doppler radar was used to obtain RHI cross sections of the

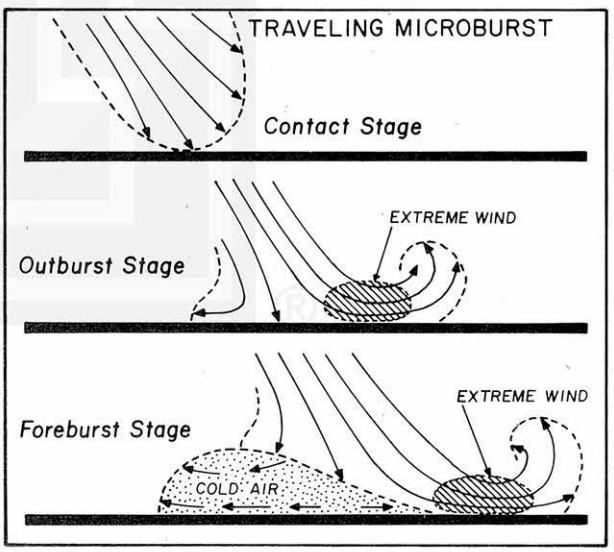

FIG. 28. Schematic diagram of a traveling microburst accompanied by an extreme wind near the ground.

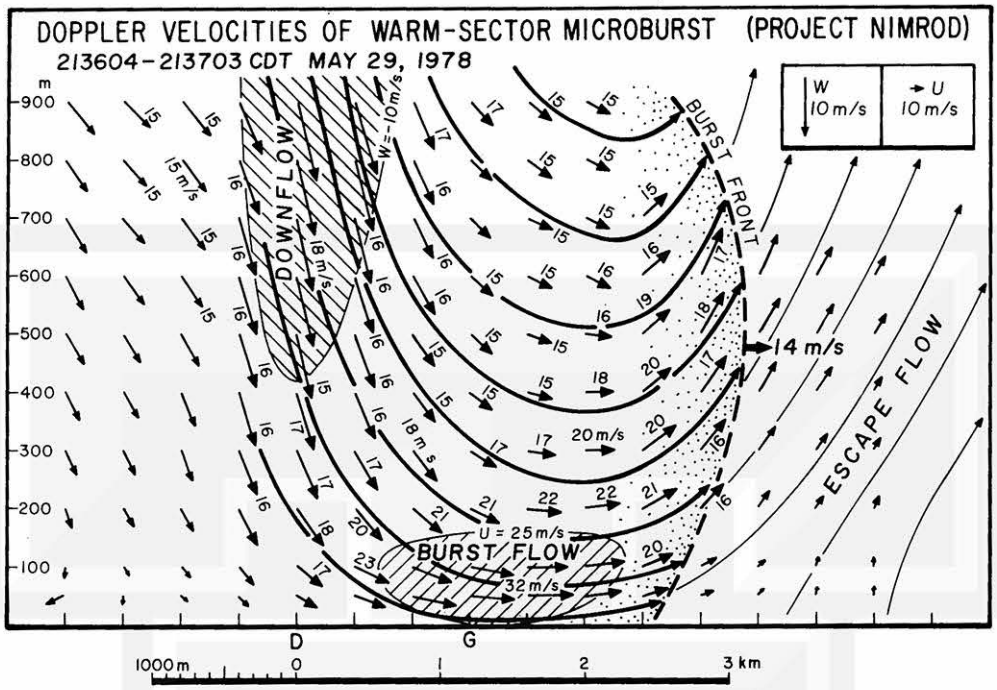

FIG. 29. Doppler velocities of a traveling microburst. The maximum wind of the horizontal outburst flow is located 50 m above the ground. An aircraft attempting to penetrate an outburst flow will encounter a tremendous increase in the tailwind as it flies out of the high-wind core.

microburst in Fig. 29 which passed within 0.8 km of the radar. The microburst was first detected at 2136 CDT, 8 km to the south-southwest of the radar. Beginning at 2141 CDT, CP-3 made a series of RHI scans between the zenith and the northwest horizon. Directions of the RHI were either upward from the horizon or downward from the zenith, depending upon the final elevation angle of the volume scans.

Fig. 31 shows in color both reflectivity (left) and velocity (right) cross sections at 1–2 min intervals. At 2140:52 CDT, Doppler velocities near the cloud top were 4–10 m s^{-1} downward while reflectivity was only 10–15 dBZ, suggesting that the descending currents extended all the way to the cloud top at 12 km above the ground. At this time the horizontal outflow had just passed the radar site.

Within 1.5 min at 2142:30 CDT, the leading edge of the downburst reached 2.5 km northwest of the radar with a 700 m depth of the outflow. Seen above the radar below 1 km height is an 8–10 m s^{-1} downward Doppler velocity associated with only a 10 dBZ reflectivity. RHI scans at 2144:28 and 2145:45 CDT show a further advancement of the outflow. The downward Doppler velocity at the cloud top decreased rapidly and finally the velocity at the cloud top turned entirely into positive in spite of the fall speeds of the particles, most likely to be ice, with 10 dBZ reflectivity.

A sequence of these RHI color pictures indicates that the vertical velocity near the cloud top was downward when a microburst in its mature stage was near the Doppler radar. Within 4–5 min, the downward motion at the cloud top reversed as the outflow near the ground expanded. It will not be possible to determine if this downburst originated at the cloud top or not. This picture sequence, nevertheless, shows that a significant descending current extended to the cloud top during the mature stage of the 29 May 1978 microburst/downburst depicted by the Project NIMROD Doppler radar.

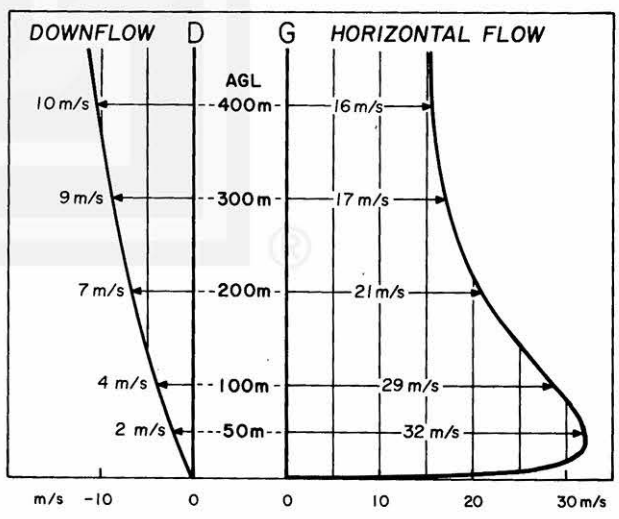

FIG. 30. Vertical distribution of horizontal flow above point G and that of downflow above point D in Fig. 29.

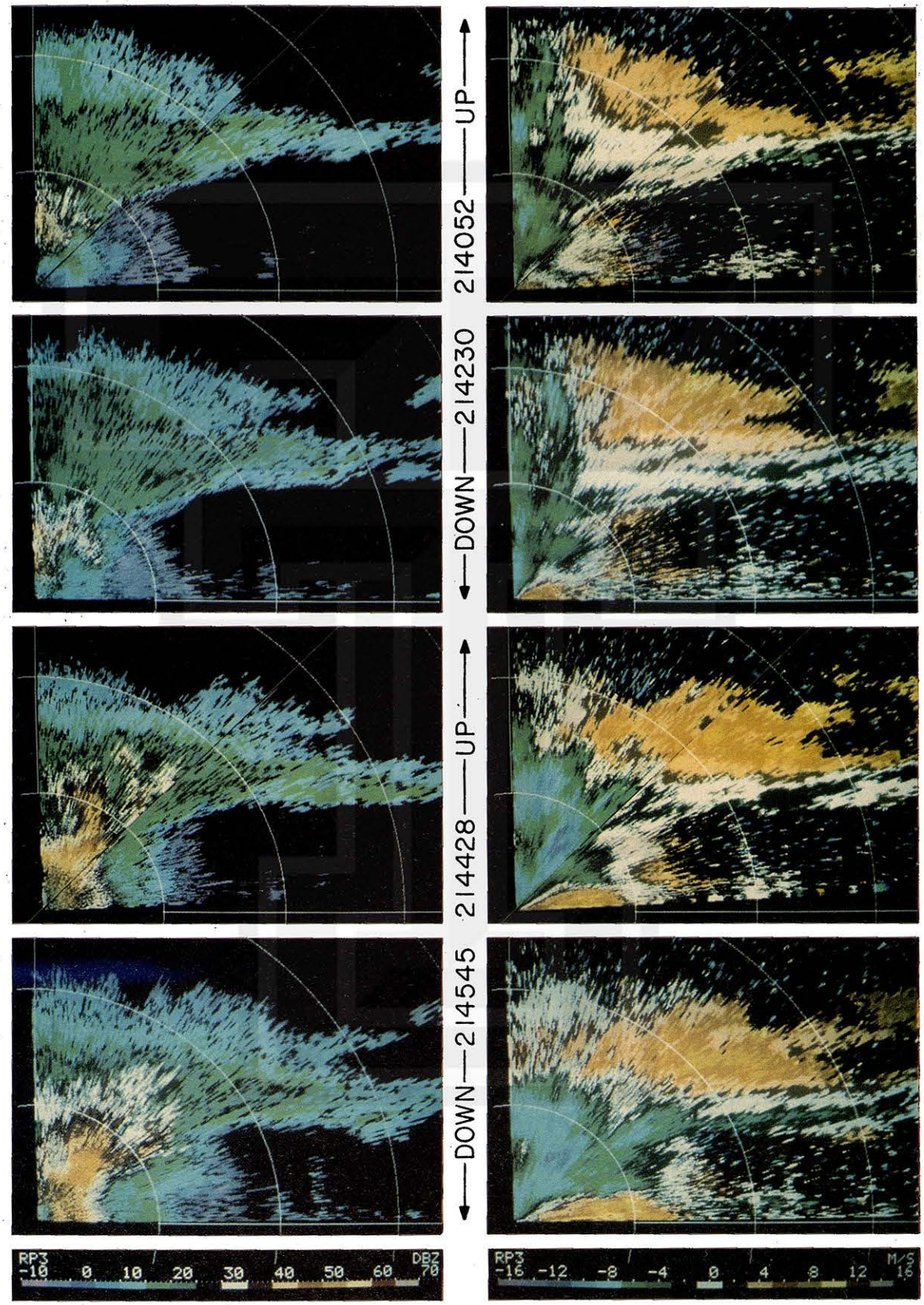

FIG. 31. RHI cross section of Yorkville, Illinois microburst on 29 May 1978 in the Project NIMROD network. Reflectivity (left) and velocity (right) are obtained by NCAR's CP-3 Doppler radar. UP and DOWN denote the direction of RHI scans with their scan-start time (h, min, s, CDT). Range markers at 5 km intervals.

TABLE 3. Relative vorticity and divergence of high and low pressure disturbances associated with thunderstorms. The Coriolis parameter f is $\sim 10^{-4}$ s^{-1} at the middle latitude.

Highs	Vorticity (s^{-1})	Divergence (s^{-1})	Life
Masohigh (anticyclone)	$-f$ to 0	0 to 0.0001	1 week or longer
Mesohigh (pressure dome)	−0.001 to +0.001	0.0001 to 0.001	3 to 18 h
Misohigh (pressure nose)	−0.01 to +0.01	0.01 to 0.1	2 to 10 min
Mosohigh (burst swath)	−0.1 to +0.1	0.1 to 1	1 min or less

Lows	Vorticity (s^{-1})	Convergence (s^{-1})	Life
Masocyclone (non-hurricane)	0 to $5f$	0 to 0.0001	3 to 10 days
Mesocyclone (supercell)	0.01 to 0.1	0.001 to 0.01	1 to 6 h
Misocyclone (tornado)	0.1 to 10	0.01 to 1	1 to 100 min
Mosocyclone (suction vortex)	1 to 10	0.1 to 10	1 to 100 s

7. Conclusions

In the context of the A-E-I-O-U planetary scales, thunderstorm-associated highs and lows were described and characterized. Results indicate that the magnitudes of vorticity and divergence tend to increase with decreasing horizontal scale (Table 3).

The maximum wind speeds induced by various highs and lows are rather difficult to estimate with reasonable accuracy. However, there are tendencies that extreme winds are accompanied by mososcale and mososcale disturbances with extreme values of vorticity and divergence (convergence).

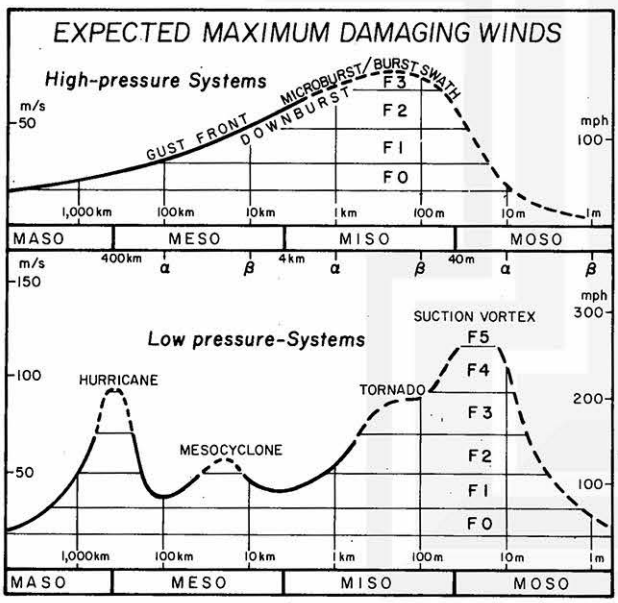

FIG. 32. Schematic distributions of expected maximum windspeeds induced by thunderstorms. The maximum winds associated with high-pressure systems are seen predominantly in misoscale outflow in microbursts and burst swaths. Maximum winds in low-pressure systems show several peaks of maximum winds corresponding to hurricanes, mesocyclones, tornadoes and suction vortices. Dashed curves denote unconfirmed wind speeds. Localized high winds beneath mesocyclones are often divergent, associated with twisting downburst.

Fig. 32 presents schematic distributions of maximum winds estimated through this research. These distributions suggest that the peak winds in downburst are experienced inside the burst swath which falls into miso-β scale. Mososcale cyclones or suction vortices appear to be the inducers of the worst winds in the tornado. Within the mososcale, however, the peak wind speeds are associated with moso-α scale, rather than with moso-β scale in which maximum winds decrease rapidly toward musoscale.

It has been shown that the parent storms of thunderstorm-induced high winds are mesoscale disturbances. The occurrences of extreme winds in misoscale and mososcale disturbances suggest the importance of the scale interactions by which the kinetic energy somehow cascades down into submesoscale airflows. Interactive researches between modelers and fact finders will provide us with the key to unlock the mystery of these multiple scales of atmospheric motion.

Acknowledgments. The research leading to the completion of this paper has been sponsored by the National Aeronautics and Space Administration under Grant NGR 14-001-008, National Oceanic and Atmospheric Administration under Grant NOAA NA80AA-D-00001, Nuclear Regulatory Commission under Contract NRC 04-74-239, and the National Science Foundation under Grant NSF/ATM 79-21260.

APPENDIX

Definition of Terms

α- and β-subscales: The larger and the smaller halves of logarithmic lengths of the generalized A-E-I-O-U scales.

Bow echo: A bow-shaped mesoscale echo, a potential inducer of strong downbursts. During the strong downburst stage, the bow echo takes the shape of a spearhead with a weak-echo channel associated with extreme winds. Prior to its dissipation, the bow echo often turns into a comma-shaped meso-α scale echo.

Burst swath: A miso-β or moso-α scale swath of extreme wind which occurs within the downburst or microburst airflow. A long and narrow burst swath often resembles the path of a tornado.

Downburst: A strong downdraft which induces an outburst of damaging winds on or near the ground. Damaging winds, either straight or curved, are highly divergent. Twisting downbursts characterized by curved streamlines are often induced by a rotating thunderstorm.

Microburst: In meteorology; a misoscale downburst with either straight or curved airflow. Some microbursts are embedded inside a mesoscale downburst while others are induced by small convective storms with rain or virga.

In aviation, a localized downdraft with its downflow speed exceeding the climb or descent rate of an aircraft (3–4 m s^{-1} at 100 m). Crosswind or tailwind shear in outburst winds of a strong microburst endangers aircraft operations near the ground.

Suction vortex: A mososcale vortex embedded inside a tornado, sometimes observable as a swirling column of dust or debris with or without a funnel cloud inside. A traveling suction vortex produces a narrow swath of extreme winds, often leaving behind a low pile of small debris along the locus of the vortex center on the ground. Some transient suction vortices remain stationary on the ground while the parent tornado aloft keeps traveling.

Tornado: A fast-rotating misocyclone accompanied by a damaging wind on or near the ground, and nearly always observable as a funnel cloud pendant from the parent cloud. The most destructive winds in the tornado occur inside the swath of one to six suction vortices which orbit around the tornado center.

REFERENCES

Agee, E. M., J. T. Snow and P. R. Clare, 1976: Multiple vortex features in the tornado cyclone and the occurrence of tornado families. *Mon. Wea. Rev.*, **104,** 552–563.

——, ——, F. S. Nickerson, P. R. Clare, C. R. Church and L. A. Schall, 1977: An observational study of the West Lafayette, Indiana Tornado of 20 March 1976. *Mon. Wea. Rev.*, **105,** 893–907.

Brandes, E. A., 1978: Mesocyclone evolution and tornadogenesis: Some observations. *Mon. Wea. Rev.*, **16,** 995–1011.

Brooks, C. F., 1922: The local, or heat thunderstorm. *Mon. Wea. Rev.*, **50,** 281–287.

Brown, J. M., and K. R. Knupp, 1980: The Iowa cyclonic-anticyclonic tornado pair and its parent thunderstorm. *Mon. Wea. Rev.*, **108,** 1626–1646.

Brown, R. A., W. C. Bumgarner, K. C. Crawford and D. Sirmans, 1971: Preliminary Doppler velocity measurements in a developing radar hook echo. *Bull. Amer. Meteor. Soc.*, **52,** 1186–1188.

Brunk, I. W., 1949: Pressure pulsations of April 11, 1944. *J. Meteor.*, **6,** 171–178.

Burgess, D. W., L. D. Hennington, R. J. Doviac and P. S. Ray, 1976: Multi-moment Doppler display for severe storm identification. *J. Appl. Meteor.*, **15,** 1302–1306.

Byers, H. R., 1959: Outline of synoptic analysis. *General Meteorology*, 3rd ed. McGraw-Hill, 363–367.

——, and R. R. Braham, Jr., 1949: *The Thunderstorm*. U.S. Govt. Printing Office, Washington, DC, 287 pp.

Emanuel K. A., 1981: A similarity theory for unsaturated downdrafts within clouds. *J. Atmos. Sci.*, **38,** 1541–1557.

Fujita, T. T., 1950: Microanalytical study of thunder nose. *Geophys. Mag. Tokyo*, **22,** 78–88.

——, 1955: Results of detailed synoptic studies of squall lines. *Tellus*, **4,** 437–451.

——, 1963: *Analytical Mesometeorology: A Review. Meteor. Monogr.*, No. 27, Amer. Meteor. Soc., 77–125.

——, 1970: Lubbock tornadoes: A study of suction spots. *Weatherwise*, **23,** 160–173.

——, 1973: Tornadoes around the world. *Weatherwise*, **26,** 56–62, 78–83.

——, 1977: Anticyclonic tornadoes. *Weatherwise*, **30,** 51–64.

——, and F. Caracena, 1977: An analysis of three weather-related aircraft accidents. *Bull. Amer. Meteor. Soc.*, **58,** 1164–1181.

——, H. Newstein and M. Tepper, 1956: Mesoanalysis—an important scale in the analysis of weather data. U.S. Govt. Printing Office, Washington, DC, 83 pp.

——, D. L. Bradbury and C. F. Van Thullenar, 1970: Palm Sunday Tornadoes of April 11, 1965. *Mon. Wea. Rev.*, **29,** 26–69.

——, K. Watanabe, K. Tsuchiya and M. Shimada, 1972: Typhoon-associated tornadoes in Japan and new evidence of suction vortices in a tornado near Tokyo. *J. Meteor. Soc. Japan*, **50,** 431–453.

Fujiwara, S., 1943: Report of thunderstorm observation project. Japan Meteor. Agency, Tokyo, 248 pp.

Garrett, R. A., and V. D. Rockney, 1962: Tornadoes in Northern Kansas, May 19, 1960. *Mon. Wea. Rev.*, **90,** 231–240.

Glossary of Meteorology, Ralph E. Huschke, Ed., 1959: American Meteorological Society, 638 pp.

Hazen, H. A., 1890: Tornadoes—a prize essay. *Amer. Meteor. J.*, **7,** 205–229.

Hobbs, P. V., Ed., 1979: Extratropical Cyclones: Progress and Research Needs, 45 pp. (Available from Atmospheric Sciences Dept., University of Washington, Seattle, 98195).

Koschmieder, H., 1955: Ergebnisse der Deutchen Böenmessungen 1939/41. Friedrich Vieweg & Sohn, Braunschweig, 148 pp.

Lemon, R. L., and C. A. Doswell III, 1979: Severe thunderstorm evolution and mesocyclone structure as related to tornadogenesis. *Mon. Wea. Rev.*, **107,** 1184–1197.

Ligda, M. G. H., 1951: Radar storm observation. *Compendium of Meteorology*, Amer. Meteor. Soc., 1265–1282.

Meaden, G. T., 1976: Tornadoes in Britain: Their intensities and distribution in space and time. *J. Meteor.*, **1,** 242–251.

Newton, C. W., 1950: Structure and mechanism of the prefrontal squall line. *J. Meteor.*, **7,** 210–222.

——, and H. R. Newton, 1959: Dynamical interactions between

large convective clouds and environment with vertical shear. *J. Meteor.*, **16**, 483–496.

Nolen, R. H., 1959: A radar pattern associated with tornadoes. *Bull. Amer. Meteor. Soc.*, **40**, 277–279.

Ogura, Y., 1963: A review of numerical modeling research on small-scale convection in the atmosphere. *Meteor. Monogr.*, No. 27, Amer. Meteor. Soc., 65–76.

Petterssen, S., 1956: Convective clouds and weather. *Weather Analysis and Forecasting*, 2nd ed., McGraw-Hill, 133–195.

Ray, P. S., 1976: Vorticity and divergence fields within tornadic storms from dual-Doppler observations. *J. Appl. Meteor.*, **15**, 879–890.

——, C. L. Ziegler and W. Bumgarner, 1980: Single- and multiple-Doppler radar observations of tornadic storms. *Mon. Wea. Rev.*, **108**, 1607–1625.

Rotunno, R., 1979: A study in tornado-like vortex dynamics. *J. Atmos. Sci.*, **36**, 140–155.

Schaffer, W., 1947: The thunderstorm high. *Bull. Amer. Meteor. Soc.*, **28**, 351–355.

Seelye, C. J., 1945: Tornadoes in New Zealand. *N.Z. J. Sci. Tech.*, **27**, 166–174.

Squires, P., 1958: Penetrative downdraught in cumuli. *Tellus*, **10**, 381–389.

Stout, G. E., and F. A. Huff, 1953: Radar records Illinois tornadogenesis. *Bull. Amer. Meteor. Soc.*, **34**, 281–284.

Suckstorff, G. A., 1938: Kaltlufterzeugung dürch Niederschlag. *Z. Meteor.*, **55**, 287–292.

Tepper, M., 1959: Mesometeorology, the link between macroscale atmospheric motions and local weather. *Bull. Amer. Meteor. Soc.*, **40**, 56–72.

Van Tassel, E. L., 1955: The North Platte valley tornado outbreak of June 27, 1955. *Mon. Wea. Rev.*, **83**, 255–264.

Williams, D. T., 1948: A surface micro study of squall-line thunderstorms. *Mon. Wea. Rev.*, **76**, 239–246.

Wilson, J., R. Carbone, H. H. Baynton and R. Serafin, 1980: Operational application of meteorological Doppler radar. *Bull. Amer. Meteor. Soc.*, **61**, 1154–1168.